SMAD4 is Critical in Suppression of *BRAF-V600E* Serrated Tumorigenesis

Kevin Tong[1], **Om A. Kothari**[1], **Katherine S. Haro**[1], **Anshuman Panda**[2], **Manisha M. Bandari**[1], **Jillian N. Carrick**[1], **Joseph J. Hur**[1], **Lanjing Zhang**[2,3], **Chang S. Chan**[4], **Jinchuan Xing**[1], **Michael L. Gatza**[2,5], **Shridar Ganesan**[2], **Michael P. Verzi**[1,2,†]

[1]Department of Genetics, Human Genetics Institute of New Jersey (HGINJ), Rutgers University, 145 Bevier Road, Piscataway, NJ 08854, USA

[2]Rutgers Cancer Institute of New Jersey (CINJ), 195 Little Albany Street, New Brunswick, NJ 08903, USA

[3]Department of Pathology, Penn Medicine Princeton Medical Center, Plainsboro, NJ, USA

[4]Department of Medicine, Rutgers Robert Wood Johnson Medical School, New Brunswick, NJ, USA.

[5]Department of Radiation Oncology, Robert Wood Johnson Medical School, New Brunswick, NJ, USA.

Abstract

BRAF-driven colorectal cancer is among the poorest prognosis subtypes of colon cancer. Previous studies suggest that *BRAF*-mutant serrated cancers frequently exhibit Microsatellite Instability (MSI) and elevated levels of WNT signaling. Loss of tumor-suppressor *Smad4* in oncogenic *BRAF-V600E* mouse models promotes rapid serrated tumor development and progression, and *SMAD4* mutations co-occur in human patient tumors with *BRAF-V600E* mutations. This study assesses the role of SMAD4 in early-stage serrated tumorigenesis. *SMAD4* loss promotes Microsatellite Stable (MSS) serrated tumors in an oncogenic *BRAF-V600E* context, providing a model for MSS serrated cancers. Inactivation of *Msh2* in these mice accelerated tumor formation, and whole exome sequencing of both MSS and MSI serrated tumors derived from these mouse models revealed that all serrated tumors developed oncogenic WNT mutations, predominantly in the WNT-effector gene *Ctnnb1* (β-catenin). Mouse models mimicking the oncogenic β-catenin mutation show that the combination three oncogenic mutations (*Ctnnb1, Braf,* and *Smad4*) are critical to drive rapid serrated dysplasia formation. Re-analysis of human tumor data reveals *BRAF-V600E* mutations co-occur with oncogenic mutations in both WNT and SMAD4/TGFβ

pathways. These findings identify SMAD4 as a critical factor in early-stage serrated cancers and helps broaden the knowledge of this rare but aggressive subset of colorectal cancer.

Introduction

Colon cancer is the 2nd-leading cause of cancer-related deaths in the United States. While ~80% of colon cancers follow a WNT-initiated adenoma-to-carcinoma pathway, approximately 20% follow the "serrated tumor pathway"- often driven by gain-of-function *BRAF* mutations[1]. Serrated tumors have the worst prognosis of colon cancers[2–5], and though these *BRAF*-driven cancers have been modeled[6–9], there remain significant gaps in the understanding of the genetic progression of serrated tumor development. CpG Island Methylator Phenotype (CIMP), Microsatellite Instability (MSI), and oncogenic WNT activation are documented steps for serrated tumorigenesis in mouse models[6,10–14], echoing observations in human tumors[15–17]. However, these mouse models require 10–12 months to form tumors[6,9,10], slowing the studies of serrated colon cancers. Furthermore, 50% of human BRAF-driven serrated tumors associated with a defect in mismatch repair and harbor Microsatellite Instability (MSI), with the remainder being Microsatellite Stable (MSS) – the latter associated with poorer prognosis [4,17,18]. The scarcity of reports using mouse models of serrated colon cancer and the inefficiency of tumor development in these models limits translational research opportunities.

Though oncogenic BRAF mutations are inefficient at generating tumors *in vivo*, loss of pro-differentiation transcription factors such as CDX2 and SMAD4 can accelerate serrated tumorigenesis[8,9]. The SMAD4/TGFβ pathway is mutated in 57% of colon tumors[19] and is associated with poor prognosis[20]. A longstanding model pits the WNT/β-catenin pathway against the SMAD4/TGFβ pathway for control of the proliferation vs. differentiation decision in the intestinal epithelium[9,21,22]. SMAD4/TGFβ signaling has also been shown to interact with the MAPK/ERK pathway – both in activating the ERK signaling cascade and Ras signaling pathway, while also being inhibited by ERK[23]. SMAD4 is often characterized as a late-stage mutation in canonical colon cancer progression models –associated with invasion and metastasis[24–28]. However, the loss of SMAD4 appears to accelerate the initiation and progression of BRAF-V600E tumors in vivo[9], suggesting an alternative pathway to serrated colon cancer progression.

This study looks to address how SMAD4/TGFβ and WNT pathways impact the progression of *BRAF-V600E* serrated colon cancers. Using mouse genetic models, we reveal that *SMAD4*-loss bypasses the MSI requirement for serrated tumor progression, and functionally demonstrate that WNT is a key driver of serrated cancers. The order of *SMAD4*-loss or WNT-activation does not appear to impact the progression of serrated lesions to high-grade dysplasias. Human tumors also exhibit a correlation between *BRAF-V600E* and mutations in WNT and *SMAD4*/TGFβ pathways. Our findings indicate that SMAD4 is a key component of serrated tumorigenesis and expand the avenues through which serrated tumors could arise in patients.

RESULTS

Loss of SMAD4 Promotes Microsatellite Stable (MSS) Tumors

As opposed to canonical adenocarcinomas initiated by oncogenic WNT pathway activation, serrated cancers are often driven by an oncogenic BRAF mutation – most commonly *BRAF-V600E*[5,19]. Several reports found that modeling the *Braf^V600E* mutation *in vivo* is inefficient at generating serrated tumors- and was attributed, in part, to the differentiation-promoting consequences of BRAF-activation in stem cells[6,7,9,10]. Thus, other factors or mutations must be required for *BRAF-V600E* serrated cancers to develop. In human colon tumors with *BRAF-V600E* driver mutations, at least 30% of patients (214/703) have a driver mutation in TGFβ-pathway associated genes – with the common driver mutations being truncations (black bars) or missense mutations (green bars) (Fig. 1A). The predominant mutation was in *SMAD4* (21% of *BRAF-V600E* patients), consistent with mouse models where loss of *SMAD4* accelerates *BRAF-V600E* tumor progression[9].

About 50% serrated tumors are deficient in Mismatch repair (MMR), leading to high frequency of Microsatellite Instability (MSI)[29]. Mouse models indicate that accumulation of MSI is an early step for serrated tumorigenesis[6,10]. Since SMAD4/TGFβ is associated with DNA damage and DNA repair response[30], perhaps loss of *SMAD4* in *BRAF^V600E/+* mice generates a favorable environment for MSI. To determine MSI status of *Smad4^KO BRAF^V600E/+* tumors, tumor organoids derived from macroscopic serrated tumors in *Smad4^KO BRAF^V600E/+ Villin-Cre^ERT2* mice[9,31–33] were collected for MSI analysis of known loci of MSI[6,34]. Epithelium from untreated littermates (wildtype) and mismatch repair deficient mice (*Msh2^KO Villin-Cre^ERT2*)[35] were used as negative and positive controls, respectively. While tissue from wildtype littermates exhibited no changes microsatellite lengths, *Msh2^KO* samples exhibited microsatellite size shift events at 50% of tested loci, indicating that the MMR deficient tissue accumulates MSI, as expected (Fig. 1B, pink boxes)[6,34,35]. For *Smad4^KO BRAF^V600E/+* tumors, 4 of the 6 tumors collected from one to four months showed no change at any of the MSI loci tested, while 2 the tumor samples collected at five and six months showed changes at 25% and 50% of loci, respectively. Because only the most mature tumor samples exhibit shifts in microsatellite sizes, these results suggest that SMAD4 does not directly impact mismatch repair, and the tumors that develop in *Smad4^KO BRAF^V600E/+* mice are primarily Microsatellite Stable (MSS).

To determine whether MSS tumors exhibit *SMAD4* loss in human patients, *BRAF-V600E* tumors (AACR GENIE)[36] were examined for *SMAD4* alterations (Fig. 1C), and patients were classified according to *SMAD4* alteration type. *BRAF-V600E* patients with oncogenic *SMAD4* alterations did not have a significantly higher tumor mutation burden than patients without oncogenic *SMAD4* (p-val = 0.13, Fig. 1C). In contrast, *BRAF-V600E* tumors harboring oncogenic mutations in other TGFβ pathway genes had a significantly higher mutation burden than the remaining *BRAF-V600E* tumors (Fig. 1D, p-val < 10^{-15}). High mutation burden is a surrogate for MSI status in colon cancer (Suppl. Fig. S1A)[19,37] which suggests that *BRAF-V600E* tumors with *SMAD4* mutations are enriched in MSS, and tumors with TGFβ pathway mutations are more likely to appear in MSI tumors. Notably, the

hotspot *TGFBR2-K128Afs*3* frameshift mutation is found within a mononucleotide repeat sequence in human which is absent in the mouse sequence; mono-nucleotide repeats are a common mutational target in MSI tumors (Suppl. Fig. S1B)[38,39]. These data suggest that loss of SMAD4 in both mouse and human patients corresponds to tumors with lower mutational burden, and links SMAD4 loss to MSS tumorigenesis.

MMR Deficiency Accelerates *BRAF*-driven Serrated Tumorigenesis

Even though SMAD4 loss does not lead to MSI (Fig. 1B), serrated tumorigenesis is greatly accelerated within the $Smad4^{KO} BRAF^{V600E/+}$ mouse model when compared to $Braf^{V600E/+}$ mice[9]. To determine whether MMR deficiency further accelerates serrated tumorigenesis, the $Msh2^{KO}$ allele[35] was incorporated into the $Smad4^{KO} BRAF^{V600E/+}$ $Villin\text{-}Cre^{ERT2}$ mouse model[9]. $Smad4^{KO} BRAF^{V600E/+} Villin\text{-}Cre^{ERT2}$ mice and $Msh2^{KO}$ $Smad4^{KO} BRAF^{V600E/+} Villin\text{-}Cre^{ERT2}$ mice were injected with tamoxifen to induce intestine-specific recombination and were collected 2–3 months post-tamoxifen treatment to assess tumor burden (Fig 2A). Macroscopic tumors were found in the intestinal tract of both $Smad4^{KO} BRAF^{V600E/+}$ and $Msh2^{KO} Smad4^{KO} BRAF^{V600E/+}$ mice (Fig. 2B, white circles). Quantification of tumor burden in the mice coincides with previous findings that $Smad4^{KO}$ $BRAF^{V600E/+}$ mice exhibit macroscopic tumors as early as two months[9]. Strikingly, the MMR deficient $Msh2^{KO} Smad4^{KO} BRAF^{V600E/+}$ mice harbored an approximate doubling of the visible tumors when compared to the $Smad4^{KO} BRAF^{V600E/+}$ mice (Fig. 2C, Student's T-Test, p-val = 0.0942), though no significant differences in tumor size were observed (Fig. 2D). Both $Smad4^{KO} BRAF^{V600E/+}$ and $Msh2^{KO} Smad4^{KO} BRAF^{V600E/+}$ tissues exhibited a jagged, "sawtooth" like epithelium, a hallmark morphology of serrated cancers[40] (Fig. 2E). Sporadic serrated dysplasias interrupted the villous epithelium. Notably, 3 of 5 $Msh2^{KO}$ $Smad4^{KO} Braf^{V600E/+}$ mice harbored tumors showing epithelial penetration into the basal layer of the intestine, indicative of invasive behavior (Fig. 2E). Loss of MSH2 results in a significant increase of dysplastic lesions (Fig. 2F, Student's T-Test, p-val = 0.005), revealing that MMR deficiency in addition to loss of SMAD4 further accelerates $BRAF^{V600E}$-driven serrated tumor development.

Serrated Tumorigenesis in $Smad4^{KO} BRAF^{V600E/+}$ mice requires activating mutations in the WNT pathway

The introduction of the $Msh2^{KO}$ alleles increases tumor numbers seen in the $Smad4^{KO}$ $BRAF^{V600E/+}$ mouse background, suggesting additional mutations are required to transition normal tissue to serrated tumors. It also is possible that the mutation(s) acquired in an MSI environment are different than those accumulated in an MSS environment. To identify these critical mutations, tumor epithelium derived from tamoxifen-treated $Smad4^{KO} BRAF^{V600E/+}$ $Villin\text{-}Cre^{ERT2}$ and $Msh2^{KO} Smad4^{KO} BRAF^{V600E/+} Villin\text{-}Cre^{ERT2}$ mice was collected for Whole Exome Sequencing (WES) (Fig. 3A). Matched tail DNA served as a reference for germline variation. Data were analyzed to identify single nucleotide variants (SNVs) and base insertions and deletions (Indels) in the tumors. $Smad4^{KO} BRAF^{V600E/+}$ tumors (n=3) averaged approximately 100 total variants (SNVs + Indels) per sample. In contrast, $Msh2^{KO} Smad4^{KO} BRAF^{V600E/+}$ tumors (n=9) had over 1000 total variants per sample (Fig. 3B, Student's T-Test, p-val < 0.0001). There was also an increase of indels in $Msh2^{KO} Smad4^{KO} BRAF^{V600E/+}$ tumor samples – consistent with $Msh2^{KO}$ mice models

(Fig. 3C, Student's T-Test, p-val = 0.0342)[35,41]. Annotation of the variants revealed that while $Smad4^{KO}$ $BRAF^{V600E/+}$ tumors averaged <10 non-synonymous mutations, $Msh2^{KO}$ $Smad4^{KO}$ $BRAF^{V600E/+}$ tumors accumulated on average 120 non-synonymous mutations within the same time frame, confirming that MMR deficiency results in a significant increase in mutational burden (Fig. 3D, Student's T-Test, p-val < 0.0001).

To identify whether independently isolated tumors would share common mutations, annotated WES data for $Smad4^{KO}$ $BRAF^{V600E/+}$ tumor organoids and $Msh2^{KO}$ $Smad4^{KO}$ $BRAF^{V600E/+}$ tumor organoids was filtered for known oncogenic mutations (Fig. 3E, blue) and truncation mutations in known cancer genes (Fig. 3E, black)[42]. In both genetic models, the majority of mutated genes were unique to a single tumor sample, suggesting that each tumor sample represented a unique tumorigenic event and not a multi-clonal population. Interestingly, all 3 $Smad4^{KO}$ $BRAF^{V600E/+}$ tumors (orange arrows), held a mutation in $Ctnnb1$ – which encodes the critical WNT effector β-catenin protein[43]. $Ctnnb1$ was also mutated in 8/9 $Msh2^{KO}$ $Smad4^{KO}$ $BRAF^{V600E/+}$ tumors (Fig 3E). The single tumor sample that was wildtype for $Ctnnb1$ harbored a nonsense mutation in another WNT-pathway gene, Apc (Suppl. Table S1). All of the $Ctnnb1$ mutations were concentrated in exon 3, at three specific codons (encoding 3 amino acids: D32, S37, and T41) (Fig. 3F). Specifically, 5/12 tumors acquired an oncogenic mutation at the T41 site, which is the predominant "hotspot" in human patients (Fig. 3G). All three mutated sites are documented oncogenic alleles of $Ctnnb1$ in human patients which stabilize β-catenin and result in elevated WNT signaling[44]. These findings reveal that $Smad4$-negative, $BRAF$-$V600E$ tissues, regardless of MSI status, all acquired oncogenic WNT mutations to progress to macroscopic tumors.

To corroborate the activation of the WNT pathway, intestinal tissue from $Smad4^{KO}$ $BRAF^{V600E/+}$ and $Msh2^{KO}$ $Smad4^{KO}$ $BRAF^{V600E/+}$ mice were stained for markers of enhanced proliferation (Ki67) and WNT activation (CD44, β-catenin)[6,7,9]. In both $Smad4^{KO}$ $BRAF^{V600E/+}$ and $Msh2^{KO}$ $Smad4^{KO}$ $BRAF^{V600E/+}$ mice, expression of these pro-growth markers is compartmentalized within the crypts in non-tumor tissue (Fig. 4A). However, dysplastic lesions found in both mouse models reveal disorganized epithelia with Ki67+ cells extending beyond the crypts and into the entirety of the lesions, consistent with previous descriptions of serrated dysplasias[6,9] (Fig 4A). Furthermore, invasive lesions identified in $Msh2^{KO}$ $Smad4^{KO}$ $BRAF^{V600E/+}$ mice reveal Ki67+ cells also penetrating through the intestinal muscle layer (Fig. 4A). As an indication that WNT may drive the ectopic proliferation, CD44 expression is highly elevated across the dysplastic lesions (and invasive regions) in both $Smad4^{KO}$ $BRAF^{V600E/+}$ and $Msh2^{KO}$ $Smad4^{KO}$ $BRAF^{V600E/+}$ mice when compared to non-tumor tissue, indicative of a high WNT environment (Fig. 4B). Similarly, β-catenin elevation is also found to extend well throughout the dysplastic and invasive lesions (Fig. 4C). RNA expression levels were also assessed for WNT pathway targets in tumor-derived organoids from each model. Wildtype organoids, $Smad4^{KO}$ $BRAF^{V600E/+}$ and $Msh2^{KO}$ $Smad4^{KO}$ $BRAF^{V600E/+}$ tumor organoids were passaged, cultured for 3 days, and collected for qRT-PCR on WNT-associated genes[6]. Relative to wildtype organoid expression levels, both $Smad4^{KO}$ $BRAF^{V600E/+}$ and $Msh2^{KO}$ $Smad4^{KO}$ $BRAF^{V600E/+}$ tumors showed a significant increase in WNT target gene transcript levels ($Ccnd1$, $Cd44$, $Epha2$, ANOVA, p-val < 0.05). Wildtype organoids, $Smad4^{KO}$ $BRAF^{V600E/+}$

and $Msh2^{KO}$ $Smad4^{KO}$ $BRAF^{V600E/+}$ tumor organoids were then cultured in media without WNT agonist R-Spondin to assess for WNT independence[24,25,45]. After 7 days, wildtype organoids were no longer viable (ANOVA, p-val = 0.0107), whereas both $Smad4^{KO}$ $BRAF^{V600E/+}$ and $Msh2^{KO}$ $Smad4^{KO}$ $BRAF^{V600E/+}$ tumors survived in media lacking R-Spondin – indicative of oncogenic WNT activation in the tumor organoids[24,25] (Fig. 4E). Tumor organoids were also assessed for acetyl-β-catenin, a transcriptionally active state of the protein[46,47]. While wildtype organoids showed almost no acetyl-β-catenin, $Smad4^{KO}$ $BRAF^{V600E/+}$ and $Msh2^{KO}$ $Smad4^{KO}$ $BRAF^{V600E/+}$ tumors show robust expression of the active form of β-catenin (Fig. 4F). Interestingly, the tumor organoids also show an elevated level of total β-catenin when compared to wildtype organoids, consistent with $Ctnnb1$ mutations in exon3 that promote protein stability[48,49] (Fig 3, Fig. 4F). These findings reveal that hyperactive WNT expression coincides with increased proliferation and supports findings that there is a requirement for WNT elevation in the progression of $BRAF$-driven tumors[6,7,10,11].

Oncogenic *BRAF* and WNT serrated dysplasias have reduction in SMAD4

Given the consistency of an oncogenic WNT mutation in $Smad4^{KO}$ $BRAF^{V600E/+}$ tumors, we wondered whether SMAD4 loss was critical for tumorigenesis, or simply predisposed the tissue to activating mutations in the WNT pathway. To test this question, an oncogenic WNT allele emulating oncogenic $Ctnnb1$ driver mutations[50] ($Ctnnb1^{Exon3/+}$) was bred into the $BRAF^{V600E/+}$ mouse model. $BRAF^{V600E/+}$ $Ctnnb1^{Exon3/+}$ $Villin\text{-}Cre^{ERT2}$ mice were injected with tamoxifen for 4 consecutive days to induce oncogenic activation of WNT and BRAF alleles. Mice were collected 6–14 days post injection and intestinal tissue was then processed for histology. $BRAF^{V600E/+}$ $Ctnnb1^{Exon3/+}$ showed broad regions of hyperplastic tissue, characterized by elongated villi and crypt structures when compared to untreated wildtype mice (Fig. 5A)[6]. Furthermore, Ki67 immunostaining of the crypt compartments revealed excess proliferation beyond the crypt compartment and extended into the villus. Immunohistochemistry of Smad4 was performed to determine if SMAD4 expression is altered. In wildtype tissue, Smad4 staining was prominent and nuclear within the intestinal epithelium. However, within the hyperplastic $BRAF^{V600E/+}$ $Ctnnb1^{Exon3/+}$ tissue, Smad4 staining appears to be more diffuse, suggesting that Smad4 expression could be reduced in the hyperplastic state (Fig. 5A). Intriguingly, no dysplastic lesions were observed within the $BRAF^{V600E/+}$ $Ctnnb1^{Exon3/+}$ $Villin\text{-}Cre^{ERT2}$ mice.

The short lifespan of tamoxifen-treated $BRAF^{V600E/+}$ $Ctnnb1^{Exon3/+}$ $Villin\text{-}Cre^{ERT2}$ mice limits the capability to model the progression of hyperplastic lesions to dysplasias. To assess more advanced stages of serrated tumor progression, the $Lgr5^{EGFP\text{-}IRES\text{-}creERT2}$ driver ($Lgr5\text{-}Cre$)[51], which is expressed in a mosaic fashion within intestinal stem cells was employed. The mosaic activation of $BRAF^{V600E/+}$ $Ctnnb1^{Exon3/+}$ allowed the animals to survive for longer periods and develop dysplastic lesions. Serrated dysplastic lesions were observed at 2 months post-tamoxifen treatment and could be assessed for SMAD4 expression. Interestingly, SMAD4 immunostaining revealed that while some dysplasias retained robust SMAD4 expression that localized to the nuclei, other dysplasias within a same mouse exhibited a loss of SMAD4 expression (Fig. 5B-C). An average of 60% of dysplastic tumors retained SMAD4 expression, and the remaining 40% of tumors lost

SMAD4 immunoreactivity (Fig. 5D). $BRAF^{V600E/+}$ $Ctnnb1^{Exon3/+}$ dysplasias were then dissected from adjacent tissue and RNA was extracted to assess $Smad4$ expression (Fig. 5E). Consistent with immunohistology, serrated dysplasias also revealed a 40% decrease in $Smad4$ RNA expression when compared to adjacent, non-tumor tissue (Fig. 5F, n=4, Student's T-Test, p-val = 0.0477). Thus, it appears that a substantial proportion of serrated tumors arising from oncogenic $BRAF$ and WNT epithelium lose SMAD4 expression. These data further implicate SMAD4 inactivation as a critical step in the development of serrated dysplasias.

Mutations in WNT, *Smad4, and BRAF*$^{V600E/+}$ combine to drive serrated dysplasia

The observed loss of SMAD4 in $BRAF^{V600E/+}$ $Ctnnb1^{Exon3/+}$ dysplasias (Fig. 5), coupled with the observation that mutations in the WNT pathway are acquired in all $Smad4^{KO}$ $BRAF^{V600E/+}$ tumors (Fig. 3), indicates that mutations in all three genes are critical for promoting serrated dysplasias. To test this, the $Ctnnb1^{Exon3/+}$ allele was integrated into the $Smad4^{KO}$ $BRAF^{V600E/+}$ background. $BRAF^{V600E/+}$ $Ctnnb1^{Exon3/+}$ or $Smad4^{KO}$ $BRAF^{V600E/+}Ctnnb1^{Exon3/+}$ (triple mutant) mice where then compared using either the *Villin-Cre* or colon specific *Cdx2-Cre* driver[8,52] (Fig. 6A). $BRAF^{V600E/+}$ $Ctnnb1^{Exon3/+}$ and $Smad4^{KO}$ $BRAF^{V600E/+}Ctnnb1^{Exon3/+}$ mice were treated with tamoxifen and compared for serrated tumorigenesis within 7-days post-injection due to rapid deterioration of health of $Smad4^{KO}$ $BRAF^{V600E/+}$ $Ctnnb1^{Exon3/+}$ *Villin-Cre* mice. When compared to untreated wildtype mice, $BRAF^{V600E/+}$ $Ctnnb1^{Exon3/+}$ tissue exhibited hyperplastic, elongated crypts with increased proliferation, as previously noted (Fig. 5). $Smad4^{KO}$ $BRAF^{V600E/+}$ $Ctnnb1^{Exon3/+}$ mutant mice also exhibited an expansion of proliferative cells and, notably, the formation of dysplasias (Fig. 6B). While serrated dysplasias were consistently found within triple mutant mice, no dysplasias were found within the untreated wildtype nor $BRAF^{V600E/+}$ $Ctnnb1^{Exon3/+}$ mice (Fig. 6C, ANOVA, p-val = 0.0004).

While the majority of tumors arose within the small-intestine, similar results were seen using the colon-restricted *Cdx2-Cre* driver. While H&E stain of the untreated wildtype mice showed normal colon structure, both $BRAF^{V600E/+}$ $Ctnnb1^{Exon3/+}$ (n=3) mutant and $Smad4^{KO}$ $BRAF^{V600E/+}$ $Ctnnb1^{Exon3/+}$ (n=5) mutant mice had larger proximal colon mucosa with hyperplastic epithelium (Suppl. Fig. S2). Furthermore, Ki67 immunohistochemistry recapitulated previous findings in the small intestine, where proliferation within the dysplastic regions extended beyond the typical crypt proliferative region found in uninjected control tissue and found within the typically differentiated compartments of the colon adjacent to the lumen (Suppl. Fig. S2). Dysplasias were found in both the $BRAF^{V600E/+}$ $Ctnnb1^{Exon3/+}$ and $Smad4^{KO}$ $BRAF^{V600E/+}$ $Ctnnb1^{Exon3/+}$ mutant mouse colons. Quantification revealed that $Smad4^{KO}$ $BRAF^{V600E/+}$ $Ctnnb1^{Exon3/+}$ mice had on average 12 dysplasias per mouse – which is significantly higher than the number of dysplasias found $BRAF^{V600E/+}$ $Ctnnb1^{Exon3/+}$ mice (Fig. 6D, ANOVA, p-val < 0.05). Taken together, these data suggest that the activation of β-catenin and loss of SMAD4 rapidly promotes the progression of BRAF-driven colon serrated dysplasias.

Finally, to lessen the burden of mutant cells on the intestinal tract, $Smad4^{KO}$ $BRAF^{V600E/+}$ $Ctnnb1^{Exon3/+}$ alleles were moved to the mosaic *Lgr5-Cre*, which allowed mice to survive

for up to 3 weeks post-tamoxifen injection (Fig. 7A). Untreated wildtype, $BRAF^{V600E/+}$ $Ctnnb1^{Exon3/+}$, and $Smad4^{KO}$ $BRAF^{V600E/+}$ $Ctnnb1^{Exon3/+}$ $Lgr5\text{-}Cre$ mutant mice were collected for serrated tumor assessment. With the extended time post-tamoxifen treatment, both $BRAF^{V600E/+}$ $Ctnnb1^{Exon3/+}$ and $Smad4^{KO}$ $BRAF^{V600E/+}$ $Ctnnb1^{Exon3/+}$ mutant mice exhibited highly serrated morphology of the intestinal epithelium and enhanced proliferation (Ki67) when compared to wildtype controls (Fig. 7B). Quantification of dysplastic lesions revealed that while $BRAF^{V600E/+}$ $Ctnnb1^{Exon3/+}$ mutant mice developed dysplastic lesions within the small intestine as previously noted (Fig. 5), $Smad4^{KO}$ $BRAF^{V600E/+}$ $Ctnnb1^{Exon3/+}$ mice had significantly more dysplasias (Fig. 7C, Student's T-Test, p-val = 0.0175). Stunningly, $Smad4^{KO}$ $Braf^{V600E/+}$ $Ctnnb1^{Exon3/+}$ mutant also exhibited invasive tumors, with epithelial cells infiltrating into the basal membrane. Neither wildtype nor $BRAF^{V600E/+}$ $Ctnnb1^{Exon3/+}$ mice developed any invasive tumors, while at least one invasive tumor was observed in 3 out of 5 $Smad4^{KO}$ $BRAF^{V600E/+}$ $Ctnnb1^{Exon3/+}$ mice (Fig. 7D, ANOVA, p-val < 0.05). These data suggest that loss of SMAD4 may be a critical step in the progression of BRAF-driven tumors, even in the presence of activating WNT mutations, and accelerates both development and progression towards invasiveness of serrated cancers.

These data suggest that loss of SMAD4 can have a substantial role in early-stage *BRAF*-driven cancers, and both oncogenic WNT and *SMAD4* mutations are critical for serrated cancers to progress to dysplasia. Thus, it is of great interest to determine whether these trends are also found in human cases. Human CRC patient data (AACR GENIE)[36] was filtered for cases that had the oncogenic *BRAF-V600E* mutation. *BRAF-V600E* cancers were analyzed for prominent mutations in both WNT (*RNF43, APC,* and *CTNNB1*) and TGFβ (*SMAD2/3/4, TGFBR2,* and *BMPR1A*) pathways[23,53–58]. Of the cases where *BRAF-V600E* and a member of the TGFβ pathway were mutated ($SMAD^{MT}$), at least 56% of the cases also had an oncogenic mutation in WNT (Fig. 7E). Conversely, when both *BRAF-V600E* and the WNT pathway were mutated, at least 37% of patients also had an oncogenic mutation in the TGFβ pathway (Fig. 7F). These findings corroborate our mouse models in which the combination of oncogenic BRAF and WNT, and loss of SMAD4, result in rapid serrated tumorigenesis.

DISCUSSION

Serrated colorectal cancer has one of the poorest prognoses of all colon cancers yet important questions regarding serrated tumor initiation and progression remain understudied. Current oncogenic *BRAF* allele mouse models are inefficient at generating tumors[6,9,10,14]. However, these models have dictated that two well documented pathways often associated with early-stage serrated cancers are CpG Island Methylator Phenotype (CIMP) and Microsatellite Instability[12,13,16,59,60]. While both mouse and human patient studies reveal that CIMP status is tightly associated with BRAF serrated cancers[10,14,15,61,62], only 50% of BRAF-driven serrated tumors are MSI[4,17,29]. Thus, modeling serrated cancers in the context of MSS and MSI would be beneficial to understand the molecular differences between the two classifications. The *BRAF-V637E* mouse model showed that the majority of serrated polyps that arose had acquired MSI-Hi status – suggesting that that MSI is critical step in the serrated tumorigenic pathway[6]. However, not all tumors were MSI, and others have shown that the *BRAF-V637E* model

also gives rise to MSS tumors[6,11]. Given that MSS serrated tumors correspond with poorer prognosis[2,3,18,59,63,64], it is imperative to model and study MSS serrated tumors.

The $Smad4^{KO}$ $BRAF^{V600E/+}$ mouse model aggressively develops serrated tumors, at least in part through facilitating tumor initiation by reducing differentiation status of the intestinal epithelium and preserving stem cells[9]. The current study reveals that the loss of SMAD4 does not appear to impact MSI status. The earliest tumors that arose in $Smad4^{KO}$ $BRAF^{V600E/+}$ mice were all MSS, contrasting with the tumors reported in the $BRAF$-$V637E$ mouse model[6]. Interestingly, human tumors harboring $BRAF^{V600E}$ and $SMAD4$ mutations accumulate fewer mutations in tumors than other oncogenic TGFβ mutations, indicative that BRAF^{V600E} and $SMAD4$ mutant tumors are more likely to be MSS in both mice and humans. These findings suggest that loss of SMAD4 bypasses the serrated tumorigenic requirement for MSI and provides a new model for MSS serrated tumors. This provides a powerful tool to study MSS and MSI serrated tumors and their genetic progress, which could identify characteristics that dictate poor prognoses in human patients. The presence or absence of the MSI status in these mice can also provide an opportunity to model therapeutics as MSI-Hi tumors are more sensitive to immune checkpoint therapies[65–71].

WNT is critical driver of Serrated Cancers

The capability to study MSS tumors with the $Smad4^{KO}$ $BRAF^{V600E/+}$ genetic mouse model grants the opportunity to compare genetic differences between how MSS or MSI tumors develop. Thus, MMR deficiency was incorporated into the $Smad4^{KO}$ $Braf^{V600E/+}$ mouse model to induce MSI and increase mutational burden. Even within 2–3 months, introduction of MSI resulted in an increase in number of tumors and a significant increase in mutational burden relative to the MSS $Smad4^{KO}$ $BRAF^{V600E/+}$ genetic mouse model, suggesting that rapid accumulation of mutations accelerates tumor initiation. However, would the mutations found in MSI tumors be different than those found in MSS tumors? Stunningly, the mutational profiles of each of the tumor organoids were unique, even those that were derived from the same mouse. Furthermore, all 12 independent serrated tumor organoid isolates acquired mutations associated with oncogenic WNT activation (predominantly within phosphorylation sites that are mutational hotspots in the $Ctnnb1$/β-catenin gene in human patients[44]) – regardless of MSI status, suggesting that oncogenic WNT is the critical mutation for serrated tumorigenesis and most other mutations are likely to be passenger events. Histology confirms that WNT signaling is indeed elevated in both MSI and MSS tumors, consistent with previous findings that $BRAF$-driven tumors have elevated WNT-expression[6,7,10,11]. The capability of tumor organoids to grow in the absence of R-Spondin and the elevated acetyl-β-catenin further supports that oncogenic WNT mutations are critical for colon cancer initiation and progression in canonical adenomas and serrated cancers[6,7,27,28,55,72,73]. Mutations which elevate WNT signaling were to be expected. However, while $Ctnnb1$ mutations in mouse models appear to be frequent[6,11], oncogenic β-catenin mutations are relatively rare in humans and it has been previously suggested that MSI patients have lower WNT expression in histological assessments[74]. Despite this, 97% of hypermutated tumors are reported to have a mutation within the WNT pathway[19], such as APC[75–77] or RNF43[78–80], with the latter being a common target in MSI-Hi tumors[79]. This strong mutational bias towards $Ctnnb1$ in mouse serrated tumors may

reflect genomic differences between human and mouse genomes and their susceptibility to mutations resulting from defective MMR[81–83], and may be of further interest to study in the future. Taken in totality, this study reveals that the commonality between serrated tumors, regardless of MSI status, is an oncogenic WNT mutation, reinforcing the notion that WNT is a critical driver of serrated tumorigenesis[6,7,9–11].

SMAD4 is a critical factor in serrated tumorigenesis.

The current study makes it clear that activation of WNT is a critical step in the $Smad4^{KO}$ $BRAF^{V600E/+}$ tumor progression to dysplasia. In $BRAF$-driven serrated cancers, WNT mutations and elevated WNT pathway expression are most frequently found in dysplastic lesions, and not as prevalent in hyperplasias, indicative that elevated WNT signaling is critical to drive forward the serrated hyperplasia-to-dysplasia transition[6,7]. It was also recently reported that $BRAF$-$V600E$ colonoids that lose $Tgfbr2$ can form tumors, though efficiency improves upon incorporating WNT-associated genes $Rnf43/p16/Znrf3$ mutations[45]. Thus, it is possible that SMAD4 loss is dispensable, and the critical mutation for serrated tumorigenesis was an oncogenic WNT driver mutation. However, the current study reveals that while $BRAF^{V600E/+}$ $Ctnnb1^{Exon3/+}$ $Villin$-Cre mice were capable of inducing hyperplasia, the tissue failed to fully transition to dysplasias before health of mice rapidly declined. When moved to a less oppressive $Lgr5$-Cre driver, despite having both pathways activated, $BRAF^{V600E/+}$ $Ctnnb1^{Exon3/+}$ mice still had a 2-month latency in the development of serrated dysplasias. Furthermore, of the serrated lesions observed, ~40% of serrated dysplasias had decreased levels of SMAD4 expression, suggesting a more critical role of SMAD4 in the transition from hyperplasia-to-dysplasia.

If SMAD4 does indeed have a critical role in the hyperplasia-to-dysplasia transition, then the combination, rather than temporal order, of mutations ($BRAF$, WNT, and $SMAD4$) may be more critical for serrated tumorigenesis. As revealed, the $Smad4^{KO}$ $BRAF^{V600E/+}$ $Ctnnb1^{Exon3/+}$ mouse model showed aggressive, and immediate, development of serrated dysplasias– substantially faster than previously documented models[6,7,9]. Furthermore, the mosaic $Smad4^{KO}$ $BRAF^{V600E/+}$ $Ctnnb1^{Exon3/+}$ $Lgr5$-Cre model revealed not only rapid development of serrated tumors, but also rapid advancement to invasion, suggesting that it is indeed the combination of $BRAF$, WNT, and $SMAD4$ mutations are the critical drivers of serrated tumorigenesis. These results reveal that loss of SMAD4 appears to have an early-stage role in serrated tumor progression, contrasting the more well documented roles as a late-stage mutation[24,26,27,84–86]. Though the scope of this study focuses on SMAD4, it is also possible that other factors associated with the SMAD4/TGFβ have been overlooked in $BRAF$ serrated cancers. Indeed, analysis of human patient cases reveals that 60% of $BRAF$-$V600E$ patient tumors have oncogenic mutations in either WNT or TGFβ pathways and are highly likely to have both. This strongly correlates with the findings in mouse models as the combination of mutations in all 3 pathways is what instantaneously generates serrated tumors. Thus, the impact of SMAD/TGFβ pathway in serrated cancer progression may be underappreciated in previous studies[6,7,10,11]. One possible reason is that the sequence of murine $Tgfbr2$ is lacking the mononucleotide repeat which is susceptible to mutation in human MSI-Hi tumors[57,87,88]. However, other TGFβ-pathway targets may also have been mutated and it has been suggested that haploinsufficiency of $SMAD4$ can

impact cancer initiation[89,90]. With the prevalence of MSI tumors in the *BRAF-V637E* mouse model, it would be of interest to assess whether alternative mutations have impacted the expression status of the TGFβ-pathway within those tumors.

The genetic mutations and temporal order of genetic mutations acquired, for colon cancer progression has been heavily studied. Multiple groups have documented specific combinations of *KRAS, APC, p53,* and *SMAD4* achieve successful organoid transplantation and eventual metastasis in mouse models[24,25,45,86,91]. These studies suggest that SMAD4 is a late-stage mutation that is critical to ultimately achieve metastasis. However, very few have documented specific order of events required for other colon cancer subtypes – particularly serrated cancers[6,8,10,14], and even fewer have studied the molecular mechanisms of SMAD4/TGFβ within a *BRAF* context[9,11,45]. Using multiple mouse models (Fig. 8A), this study reveals SMAD4 loss as a critical step in early-stage hyperplasia-to-dysplasia transition in serrated cancers – especially for the MSS subtype (Fig. 8B). The revelation that SMAD4 has a key role in suppressing the hyperplasia-to-dysplasia transition would have far-reaching implications in how SMAD4/TGFβ regulates and maintains the homeostatic intestinal epithelium and may also provide further insight into how SMAD4 impacts the later stages of cancer progression in tumor invasion and metastasis. Further studies into the molecular mechanisms of how WNT, SMAD4/TGFβ, and BRAF pathways interact and dictate intestinal homeostasis would be compelling and may provide more insight into this rare, but deadly, class of cancers.

METHODS

Animals

Animal experiments were conducted in accordance with Rutgers University IACUC. Mice strains are listed in Table S3. Mice 6–8 weeks of age were treated with intraperitoneal injection of tamoxifen (1mg/20g), for four consecutive days unless stated otherwise. At least 3 mice per biological condition were collected (sex random) for histological assays. Treatment groups were non-blinded.

Analysis of human data:

Known oncogenic mutations in *CTNNB1* were identified in all human colorectal cancer patients (irrespective of BRAF status) from the AACR GENIE database[36] (https://genie.cbioportal.org/) and visualized them using MutationMapper (cBioPortal)[92] and IGV[93,94]. The *BRAF^{V600E}* mutant subset of these patients were analyzed further, and known oncogenic alterations in TGFβ pathway (*SMAD4, TGFBR2, SMAD2, SMAD3, BMPR1A*) and WNT pathway (*RNF43, APC, CTNNB1*) were identified and visualized using OncoPrinter (cBioPortal). Within the *BRAF^{V600E}* mutant subset, oncogenic mutations in *SMAD4* and *TGFBR2* were visualized using MutationMapper, and mutation count was compared between tumors with/without oncogenic alteration in *SMAD4* as well as tumors known/not known to have oncogenic mutation in other TGFβ pathway genes (2-sided Wilcoxon rank-sum test). To supplement these results, mutation count was also compared between MSI and MSS (CIN, GS, POLE) colorectal cancers (irrespective of BRAF

status) in TCGA pan-cancer atlas dataset[19] (https://www.cbioportal.org/study/summary?id=coadread_tcga_pan_can_atlas_2018).

Organoid Culture

Crypt-derived organoids were isolated from duodenum and cultured in Cultrex reduced growth factor matrix R1 (BME-R1) (Trevigen) according to established methods[95]. Tumor organoids were derived from macroscopic tumors tissue found in $Smad4^{KO} BRAF^{V600E/+}$ $Villin$-Cre^{ERT2} and $Msh2^{KO} SMAD4^{KO} BRAF^{V600E/+} Villin$-$Cre^{ERT2}$ mice according to established methods[96]. An average of 100 organoids per biological replicate were seeded in 25μl of matrix with 1x Crypt Culture Media (CCM) consisting of Basic Crypt Media (BCM): Advanced DMEM/F12 (Gibco), 1% Penicillin/Streptomycin, 2mM Glutamax, 10mM HEPES (Life Technologies) supplemented with 50 ng/ml EGF (R&D), 100 ng/ml Noggin (Peprotech), A/-acetyl-l-cysteine 1 μM (Sigma-Aldrich), R-Spondin CM 2.5% (v/v), 1× N2, 1× B27 (Life Technologies).

To assess viability and WNT independence of organoids, wildtype organoids and $Smad4^{KO}$ $BRAF^{V600E/+} Villin$-Cre^{ERT2} and $Msh2^{KO} SMAD4^{KO} BRAF^{V600E/+} Villin$-$Cre^{ERT2}$ tumor organoids were passaged and cultured in CCM for 2 days. Organoids were assessed for viability and then were cultured in either complete CCM or CCM without R-Spondin for 7 days, replacing respective media every 2 days. Viability was calculated based on remaining viable organoids over initial organoid counts prior to removal of R-Spondin from media.

Microsatellite Analysis

Organoids were passaged and cultured for 3 days prior to collection. Organoid and matched mouse tail genomic DNA was extracted using QIAamp DNA Extraction Kit (QIAGEN). Extracted DNA was amplified via PCR. MSI using fluorescent PCR primers against Microsatellite target sequences[6,34]. Following PCR for the specific markers, the PCR products were purified using a QIAquick PCR Purification Kit (QIAGEN). Samples were submitted for Fragment Analysis (GENEWIZ). Data were visualized using ThermoFisher Cloud Microsatellite Analysis, on which electropherograms were plotted for comparison. Electropherograms were compared by observing the same read lengths for each sample. If 40% of markers between tail and tumor sample showed a change in sequence, the tumor was scored as microsatellite instable – high. If less than 40% of markers showed a change in sequence, the tumor was scored as microsatellite instable – low. Finally, if none of the markers showed a change in sequence, the tumor was scored as microsatellite stable[6].

Immunohistochemistry

Mouse intestines were collected and fixed overnight at 4°C in a 4% paraformaldehyde solution, and then carefully sectioned into 5μm paraffin sections. Sectioned slides were treated with 10mM sodium citrate to be put into a pressure cooker for antigen retrieval. Slides were quenched in 0.5% peroxidase for 20 minutes, washed, permeabilized in 5% Triton X-100 (in 1× PBS) for 5 minutes, blocked in 5% Fetal Bovine Serum (FBS) for 1 hour, and incubated overnight at 4°C with primary antibodies (Suppl. Table S2). Slides were developed using 0.05% DAB and 0.015% hydrogen peroxide in 0.1 M Tris. Secondary antibodies (Rabbit, 1:300; Rat, 1:300) (Vector Labs) alongside the ABC Vectastain HRP

Kit (Vector Labs) was used to develop the immunostain. Slides were counterstained with Hematoxylin.

Histology and Scoring

Serrated dysplasias were identified based on morphology (H&E) and proliferation (KI67) in swiss roll sections containing small intestine. Specifically, serrated lesions with dysplasia were defined as extended protrusions from the epithelial-lumen interface that shows KI67-positive cells throughout the elongated crypt. Invasive tumors were identified based on the disturbance of the muscle layer in which proliferation will spread past the normal boundary and into the villi. A single swiss roll section was counted for serrated lesions per mouse. Hyperplastic regions were identified based on crypts extending past normal length. $BRAF^{V600E/+} Ctnnb1^{Exon3/+} Lgr5\text{-}Cre$ dysplasias were sorted based on size, only tumors filling more than 50% of the 10x field of view were counted. These tumors were than grouped based on their SMAD4 expression levels. SMAD4 Negative tumors were identified based lack of brown nuclear staining. SMAD4 Positive tumors were identified based the concentration of brown nuclear staining.

Whole Exome Sequencing and Analysis

Tumor organoids were derived from $Smad4^{KO} BRAF^{V600E/+} Villin\text{-}Cre^{ERT2}$ and $Msh2^{KO} Smad4^{KO} BRAF^{V600E/+} Villin\text{-}Cre^{ERT2}$ intestinal tumors and propagated to ensure sufficient DNA could be extracted for sequencing. DNA was extracted from tumor organoids and matched tails using DNeasy Blood & Tissue Kit (QIAGEN). Samples were submitted for Whole Exome Sequencing (WES) (GENEWIZ). Tumor and tail raw files were aligned using BWA-MEM (0.7.17)[97] to the mouse reference genome (mm10) and processed using GATK Best Practices[98] and mouse analysis pipelines[99]. Briefly, aligned reads were processed through Mutect2, and the VCF output file would be run through and SNPSift filter (GalaxyTools)[100] using recommended settings[99]. Variants were then filtered further to select only high-quality tumor variants, with an allele frequency > 0.1 (FILTER = 'PASS' & GEN[Tumor].AF => 0.1), and sufficient allelic depth (GEN[Tumor].AD[1] >=3 & GEN[Normal].AD[1] = 0, GEN[Tumor].AD[0] + GEN[Tumor].AD[1]) => 10). Filtered calls were annotated using ENSEMBL VEP[101]. Non-coding variants and synonymous variants were omitted from the resulting data to finalize the resulting gene list. Mouse VCF files were converted to MAF files using vcf2maf (https://github.com/mskcc/vcf2maf), and OncoKB[42] (https://github.com/oncokb/oncokb-annotator) was used to identify mutations that are known to be oncogenic. Truncating (e.g. frameshift, nonsense, splice etc.) mutations in other cancer genes were identified by restricting the MAF files to known cancer genes (https://www.oncokb.org/cancerGenes). Mutations known to be oncogenic, and truncating mutations in other cancer genes, were both visualized using OncoPrinter (cBioPortal). The oncogenic mutations in CTNNB1 were visualized using MutationMapper (cBioPortal) and IGV. Unlike vcf2maf and IGV, the remaining tools were designed for human gene identification. Sequence Read Archive (SRA) BioProject: PRJNA751886.

qPCR and Analysis

Organoids were passaged and cultured in 1x CCM for 3days in Matrigel as above. Organoids were collected and placed into Trizol. RNA was extracted using RNeasy Kit

(QIAGEN). For tumor dissections and scrapes, three 10μm slides of paraffin embedded tissue were stained with Hematoxylin & Eosin. Tumors were dissected away from adjacent tissue and collected. RNA was extracted using FFPE RNeasy Kit (QIAGEN). RNA was quantified by Nanodrop. 500ng of RNA was converted to cDNA using Superscript III (Thermo). qPCR was performed and cT values were normalized to housekeeping genes *Hprt* and *Tubb5*.

Western Blot

Wildtype organoids and $Smad4^{KO} BRAF^{V600E/+} Villin-Cre^{ERT2}$ and $Msh2^{KO} SMAD4^{KO} BRAF^{V600E/+} Villin-Cre^{ERT2}$ tumor organoids were passaged and cultured in CCM for 3 days. Organoids were collected, washed in cold 1x PBS (Gibco) to remove Matrigel. Cells were then lysed to extract for protein using RIPA Lysis Buffer (50 mM Tris-HCl pH 8.0, 150 mM NaCl, 1% NP-40, 0.5% Na-deoxycholate, 0.1% SDS, protease inhibitor cocktails, and phosphatase inhibitors). Immunodetection was performed using antibodies against Acetyl-β-catenin (Cell Signaling, 1:500) and GAPDH (SantaCruz, 1:5000) with respective secondary antibodies linked to HRP (Suppl. Table S2). Blot was then stripped with Restore PLUS Western Blot Stripping Buffer (Thermo Scientific) and probed for β-catenin (Santa Cruz, 1:2000).

Statistical Analysis

Data are presented as mean ± SEM and graphed using Prism (v8.4), with individual replicates plotted. Two-sided Student T-test was used as part of the Macroscopic Tumor Count, Total Variants in Tumors Count and Number of Gene Mutations in Tumors Count. Two-way ANOVA was used as part of the Fold Change/WT Counts, Serrated Dysplasias in *Villin-Cre*, Serrated Dysplasias in *Cdx2-Cre*, Serrated Dysplasias by Day 21, Invasive Tumor in *Lgr5-Cre* models, and WNT Independent Growth of Organoids.

Supplementary Material

Refer to Web version on PubMed Central for supplementary material.

Acknowledgements

References

1. Rex DK, Ahnen DJ, Baron JA, Batts KP, Burke CA, Burt RW et al. Serrated lesions of the colorectum: review and recommendations from an expert panel. Am J Gastroenterol 2012; 107: 1315–1329; quiz 1314, 1330. [PubMed: 22710576]

2. Chouhan H, Sammour T, M LT, J WM. Prognostic significance of BRAF mutation alone and in combination with microsatellite instability in stage III colon cancer. Asia Pac J Clin Oncol 2019; 15: 69–74.

3. Samowitz WS, Sweeney C, Herrick J, Albertsen H, Levin TR, Murtaugh MA et al. Poor survival associated with the BRAF V600E mutation in microsatellite-stable colon cancers. Cancer Res 2005; 65: 6063–6069. [PubMed: 16024606]

4. Taieb J, Le Malicot K, Shi Q, Penault-Llorca F, Bouche O, Tabernero J et al. Prognostic Value of BRAF and KRAS Mutations in MSI and MSS Stage III Colon Cancer. J Natl Cancer Inst 2017; 109.

5. Yamane L, Scapulatempo-Neto C, Reis RM, Guimaraes DP. Serrated pathway in colorectal carcinogenesis. World J Gastroenterol 2014; 20: 2634–2640. [PubMed: 24627599]

6. Rad R, Cadinanos J, Rad L, Varela I, Strong A, Kriegl L et al. A genetic progression model of Braf(V600E)-induced intestinal tumorigenesis reveals targets for therapeutic intervention. Cancer cell 2013; 24: 15–29. [PubMed: 23845441]

7. Riemer P, Sreekumar A, Reinke S, Rad R, Schafer R, Sers C et al. Transgenic expression of oncogenic BRAF induces loss of stem cells in the mouse intestine, which is antagonized by beta-catenin activity. Oncogene 2015; 34: 3164–3175. [PubMed: 25109331]

8. Sakamoto N, Feng Y, Stolfi C, Kurosu Y, Green M, Lin J et al. BRAF(V600E) cooperates with CDX2 inactivation to promote serrated colorectal tumorigenesis. Elife 2017; 6.

9. Tong K, Pellon-Cardenas O, Sirihorachai VR, Warder BN, Kothari OA, Perekatt AO et al. Degree of Tissue Differentiation Dictates Susceptibility to BRAF-Driven Colorectal Cancer. Cell Rep 2017; 21: 3833–3845. [PubMed: 29281831]

10. Tao Y, Kang B, Petkovich DA, Bhandari YR, In J, Stein-O'Brien G et al. Aging-like Spontaneous Epigenetic Silencing Facilitates Wnt Activation, Stemness, and Braf(V600E)-Induced Tumorigenesis. Cancer cell 2019; 35: 315–328 e316. [PubMed: 30753828]

11. Kane AM, Fennell LJ, Liu C, Borowsky J, McKeone DM, Bond CE et al. Alterations in signaling pathways that accompany spontaneous transition to malignancy in a mouse model of BRAF mutant microsatellite stable colorectal cancer. Neoplasia 2020; 22: 120–128. [PubMed: 31935636]

12. Kambara T, Simms LA, Whitehall VL, Spring KJ, Wynter CV, Walsh MD et al. BRAF mutation is associated with DNA methylation in serrated polyps and cancers of the colorectum. Gut 2004; 53: 1137–1144. [PubMed: 15247181]

13. Tanaka H, Deng G, Matsuzaki K, Kakar S, Kim GE, Miura S et al. BRAF mutation, CpG island methylator phenotype and microsatellite instability occur more frequently and concordantly in mucinous than non-mucinous colorectal cancer. Int J Cancer 2006; 118: 2765–2771. [PubMed: 16381005]

14. Carragher LA, Snell KR, Giblett SM, Aldridge VS, Patel B, Cook SJ et al. V600EBraf induces gastrointestinal crypt senescence and promotes tumour progression through enhanced CpG methylation of p16INK4a. EMBO Mol Med 2010; 2: 458–471. [PubMed: 20941790]

15. Fernando WC, Miranda MS, Worthley DL, Togashi K, Watters DJ, Leggett BA et al. The CIMP Phenotype in BRAF Mutant Serrated Polyps from a Prospective Colonoscopy Patient Cohort. Gastroenterol Res Pract 2014; 2014: 374926. [PubMed: 24812557]

16. Hinoue T, Weisenberger DJ, Pan F, Campan M, Kim M, Young J et al. Analysis of the association between CIMP and BRAF in colorectal cancer by DNA methylation profiling. PLoS One 2009; 4: e8357. [PubMed: 20027224]

17. Seppala TT, Bohm JP, Friman M, Lahtinen L, Vayrynen VM, Liipo TK et al. Combination of microsatellite instability and BRAF mutation status for subtyping colorectal cancer. Br J Cancer 2015; 112: 1966–1975. [PubMed: 25973534]

18. Yang Y, Wang D, Jin L, Wu G, Bai Z, Wang J et al. Prognostic value of the combination of microsatellite instability and BRAF mutation in colorectal cancer. Cancer Manag Res 2018; 10: 3911–3929. [PubMed: 30310312]

19. Cancer Genome Atlas N Comprehensive molecular characterization of human colon and rectal cancer. Nature 2012; 487: 330–337. [PubMed: 22810696]

20. Yan P, Klingbiel D, Saridaki Z, Ceppa P, Curto M, McKee TA et al. Reduced Expression of SMAD4 Is Associated with Poor Survival in Colon Cancer. Clin Cancer Res 2016; 22: 3037–3047. [PubMed: 26861460]

21. Freeman TJ, Smith JJ, Chen X, Washington MK, Roland JT, Means AL et al. Smad4-mediated signaling inhibits intestinal neoplasia by inhibiting expression of beta-catenin. Gastroenterology 2012; 142: 562–571 e562. [PubMed: 22115830]

22. Perekatt AO, Shah PP, Cheung S, Jariwala N, Wu A, Gandhi V et al. SMAD4 Suppresses WNT-Driven Dedifferentiation and Oncogenesis in the Differentiated Gut Epithelium. Cancer Res 2018; 78: 4878–4890. [PubMed: 29986996]

23. Chapnick DA, Warner L, Bernet J, Rao T, Liu X. Partners in crime: the TGFbeta and MAPK pathways in cancer progression. Cell Biosci 2011; 1: 42. [PubMed: 22204556]

24. Fumagalli A, Drost J, Suijkerbuijk SJ, van Boxtel R, de Ligt J, Offerhaus GJ et al. Genetic dissection of colorectal cancer progression by orthotopic transplantation of engineered cancer organoids. Proc Natl Acad Sci U S A 2017; 114: E2357–E2364. [PubMed: 28270604]

25. Roper J, Tammela T, Cetinbas NM, Akkad A, Roghanian A, Rickelt S et al. In vivo genome editing and organoid transplantation models of colorectal cancer and metastasis. Nat Biotechnol 2017; 35: 569–576. [PubMed: 28459449]

26. Tian X, Du H, Fu X, Li K, Li A, Zhang Y. Smad4 restoration leads to a suppression of Wnt/beta-catenin signaling activity and migration capacity in human colon carcinoma cells. Biochem Biophys Res Commun 2009; 380: 478–483. [PubMed: 19284991]

27. Fearon ER, Vogelstein B. A genetic model for colorectal tumorigenesis. Cell 1990; 61: 759–767. [PubMed: 2188735]

28. Vogelstein B, Fearon ER, Hamilton SR, Kern SE, Preisinger AC, Leppert M et al. Genetic alterations during colorectal-tumor development. N Engl J Med 1988; 319: 525–532. [PubMed: 2841597]

29. Venderbosch S, Nagtegaal ID, Maughan TS, Smith CG, Cheadle JP, Fisher D et al. Mismatch repair status and BRAF mutation status in metastatic colorectal cancer patients: a pooled analysis of the CAIRO, CAIRO2, COIN, and FOCUS studies. Clin Cancer Res 2014; 20: 5322–5330. [PubMed: 25139339]

30. Liu Q, Lopez K, Murnane J, Humphrey T, Barcellos-Hoff MH. Misrepair in Context: TGFbeta Regulation of DNA Repair. Front Oncol 2019; 9: 799. [PubMed: 31552165]

31. el Marjou F, Janssen KP, Chang BH, Li M, Hindie V, Chan L et al. Tissue-specific and inducible Cre-mediated recombination in the gut epithelium. Genesis 2004; 39: 186–193. [PubMed: 15282745]

32. Dankort D, Filenova E, Collado M, Serrano M, Jones K, McMahon M. A new mouse model to explore the initiation, progression, and therapy of BRAFV600E-induced lung tumors. Genes & development 2007; 21: 379–384. [PubMed: 17299132]

33. Yang X, Li C, Herrera PL, Deng CX. Generation of Smad4/Dpc4 conditional knockout mice. Genesis 2002; 32: 80–81. [PubMed: 11857783]

34. Kabbarah O, Mallon MA, Pfeifer JD, Edelmann W, Kucherlapati R, Goodfellow PJ. A panel of repeat markers for detection of microsatellite instability in murine tumors. Mol Carcinog 2003; 38: 155–159. [PubMed: 14639654]

35. Kucherlapati MH, Lee K, Nguyen AA, Clark AB, Hou H Jr., Rosulek A et al. An Msh2 conditional knockout mouse for studying intestinal cancer and testing anticancer agents. Gastroenterology 2010; 138: 993–1002 e1001. [PubMed: 19931261]

36. Consortium APG. AACR Project GENIE: Powering Precision Medicine through an International Consortium. Cancer Discov 2017; 7: 818–831. [PubMed: 28572459]

37. Panda A, Betigeri A, Subramanian K, Ross JS, Pavlick DC, Ali S et al. Identifying a Clinically Applicable Mutational Burden Threshold as a Potential Biomarker of Response to Immune Checkpoint Therapy in Solid Tumors. JCO Precis Oncol 2017; 2017.

38. Biswas S, Trobridge P, Romero-Gallo J, Billheimer D, Myeroff LL, Willson JK et al. Mutational inactivation of TGFBR2 in microsatellite unstable colon cancer arises from the cooperation of genomic instability and the clonal outgrowth of transforming growth factor beta resistant cells. Genes Chromosomes Cancer 2008; 47: 95–106. [PubMed: 17985359]

39. Bacher JW, Abdel Megid WM, Kent-First MG, Halberg RB. Use of mononucleotide repeat markers for detection of microsatellite instability in mouse tumors. Mol Carcinog 2005; 44: 285–292. [PubMed: 16240453]

40. Leggett B, Whitehall V. Role of the serrated pathway in colorectal cancer pathogenesis. Gastroenterology 2010; 138: 2088–2100. [PubMed: 20420948]

41. Taketo MM, Edelmann W. Mouse models of colon cancer. Gastroenterology 2009; 136: 780–798. [PubMed: 19263594]

42. Chakravarty D, Gao J, Phillips SM, Kundra R, Zhang H, Wang J et al. OncoKB: A Precision Oncology Knowledge Base. JCO Precis Oncol 2017; 2017.

43. MacDonald BT, Tamai K, He X. Wnt/beta-catenin signaling: components, mechanisms, and diseases. Dev Cell 2009; 17: 9–26. [PubMed: 19619488]

44. Provost E, Yamamoto Y, Lizardi I, Stern J, D'Aquila TG, Gaynor RB et al. Functional correlates of mutations in beta-catenin exon 3 phosphorylation sites. J Biol Chem 2003; 278: 31781–31789. [PubMed: 12799363]

45. Lannagan TRM, Lee YK, Wang T, Roper J, Bettington ML, Fennell L et al. Genetic editing of colonic organoids provides a molecularly distinct and orthotopic preclinical model of serrated carcinogenesis. Gut 2019; 68: 684–692. [PubMed: 29666172]

46. Chen X, Wang C, Jiang Y, Wang Q, Tao Y, Zhang H et al. Bcl-3 promotes Wnt signaling by maintaining the acetylation of beta-catenin at lysine 49 in colorectal cancer. Signal Transduct Target Ther 2020; 5: 52. [PubMed: 32355204]

47. Wolf D, Rodova M, Miska EA, Calvet JP, Kouzarides T. Acetylation of beta-catenin by CREB-binding protein (CBP). J Biol Chem 2002; 277: 25562–25567. [PubMed: 11973335]

48. Liu C, Li Y, Semenov M, Han C, Baeg GH, Tan Y et al. Control of beta-catenin phosphorylation/degradation by a dual-kinase mechanism. Cell 2002; 108: 837–847. [PubMed: 11955436]

49. Xia J, Urabe K, Moroi Y, Koga T, Duan H, Li Y et al. beta-Catenin mutation and its nuclear localization are confirmed to be frequent causes of Wnt signaling pathway activation in pilomatricomas. J Dermatol Sci 2006; 41: 67–75. [PubMed: 16378715]

50. Harada N, Tamai Y, Ishikawa T, Sauer B, Takaku K, Oshima M et al. Intestinal polyposis in mice with a dominant stable mutation of the beta-catenin gene. EMBO J 1999; 18: 5931–5942. [PubMed: 10545105]

51. Barker N, van Es JH, Kuipers J, Kujala P, van den Born M, Cozijnsen M et al. Identification of stem cells in small intestine and colon by marker gene Lgr5. Nature 2007; 449: 1003–1007. [PubMed: 17934449]

52. Hinoi T, Akyol A, Theisen BK, Ferguson DO, Greenson JK, Williams BO et al. Mouse model of colonic adenoma-carcinoma progression based on somatic Apc inactivation. Cancer Res 2007; 67: 9721–9730. [PubMed: 17942902]

53. de Sousa EM, Vermeulen L, Richel D, Medema JP. Targeting Wnt signaling in colon cancer stem cells. Clin Cancer Res 2011; 17: 647–653. [PubMed: 21159886]

54. Polakis P Wnt signaling in cancer. Cold Spring Harb Perspect Biol 2012; 4.

55. Schatoff EM, Leach BI, Dow LE. Wnt Signaling and Colorectal Cancer. Curr Colorectal Cancer Rep 2017; 13: 101–110. [PubMed: 28413363]

56. Gotovac JR, Fujihara KM, Phillips WA, Clemons NJ. TGF-beta signaling and its targeted therapy in gastrointestinal cancers. Discov Med 2018; 26: 103–112. [PubMed: 30399328]

57. Kim SJ, Im YH, Markowitz SD, Bang YJ. Molecular mechanisms of inactivation of TGF-beta receptors during carcinogenesis. Cytokine Growth Factor Rev 2000; 11: 159–168. [PubMed: 10708963]

58. Yang G, Yang X. Smad4-mediated TGF-beta signaling in tumorigenesis. Int J Biol Sci 2010; 6: 1–8. [PubMed: 20087440]

59. Ogino S, Nosho K, Kirkner GJ, Kawasaki T, Meyerhardt JA, Loda M et al. CpG island methylator phenotype, microsatellite instability, BRAF mutation and clinical outcome in colon cancer. Gut 2009; 58: 90–96. [PubMed: 18832519]

60. Jass JR. Classification of colorectal cancer based on correlation of clinical, morphological and molecular features. Histopathology 2007; 50: 113–130. [PubMed: 17204026]

61. Ang PW, Li WQ, Soong R, Iacopetta B. BRAF mutation is associated with the CpG island methylator phenotype in colorectal cancer from young patients. Cancer Lett 2009; 273: 221–224. [PubMed: 18778891]

62. Weisenberger DJ, Siegmund KD, Campan M, Young J, Long TI, Faasse MA et al. CpG island methylator phenotype underlies sporadic microsatellite instability and is tightly associated with BRAF mutation in colorectal cancer. Nat Genet 2006; 38: 787–793. [PubMed: 16804544]

63. Guo TA, Wu YC, Tan C, Jin YT, Sheng WQ, Cai SJ et al. Clinicopathologic features and prognostic value of KRAS, NRAS and BRAF mutations and DNA mismatch repair status: A single-center retrospective study of 1,834 Chinese patients with Stage I-IV colorectal cancer. Int J Cancer 2019; 145: 1625–1634. [PubMed: 31162857]

64. Sinicrope FA. Evaluating the Combination of Microsatellite Instability and Mutation in BRAF as Prognostic Factors for Patients With Colorectal Cancer. Clin Gastroenterol Hepatol 2019; 17: 391–394. [PubMed: 29966708]

65. Chang L, Chang M, Chang HM, Chang F. Microsatellite Instability: A Predictive Biomarker for Cancer Immunotherapy. Appl Immunohistochem Mol Morphol 2018; 26: e15–e21. [PubMed: 28877075]

66. Ganesh K, Stadler ZK, Cercek A, Mendelsohn RB, Shia J, Segal NH et al. Immunotherapy in colorectal cancer: rationale, challenges and potential. Nat Rev Gastroenterol Hepatol 2019; 16: 361–375. [PubMed: 30886395]

67. Zhao P, Li L, Jiang X, Li Q. Mismatch repair deficiency/microsatellite instability-high as a predictor for anti-PD-1/PD-L1 immunotherapy efficacy. J Hematol Oncol 2019; 12: 54. [PubMed: 31151482]

68. Ando Y, Yamauchi M, Suehiro Y, Yamaoka K, Kosaka Y, Fuji Y et al. Complete response to pembrolizumab in advanced hepatocellular carcinoma with microsatellite instability. Clin J Gastroenterol 2020; 13: 867–872. [PubMed: 32020539]

69. Andre T, Shiu KK, Kim TW, Jensen BV, Jensen LH, Punt C et al. Pembrolizumab in Microsatellite-Instability-High Advanced Colorectal Cancer. N Engl J Med 2020; 383: 2207–2218. [PubMed: 33264544]

70. Barata P, Agarwal N, Nussenzveig R, Gerendash B, Jaeger E, Hatton W et al. Clinical activity of pembrolizumab in metastatic prostate cancer with microsatellite instability high (MSI-H) detected by circulating tumor DNA. J Immunother Cancer 2020; 8.

71. Das S, Allen A, Berlin J. Immunotherapy After Immunotherapy: Response Rescue in a Patient With Microsatellite Instability-high Colorectal Cancer Post-Pembrolizumab. Clin Colorectal Cancer 2020; 19: 137–140. [PubMed: 32146081]

72. Basu S, Haase G, Ben-Ze'ev A. Wnt signaling in cancer stem cells and colon cancer metastasis. F1000Res 2016; 5.

73. Zhan T, Rindtorff N, Boutros M. Wnt signaling in cancer. Oncogene 2017; 36: 1461–1473. [PubMed: 27617575]

74. Panarelli NC, Vaughn CP, Samowitz WS, Yantiss RK. Sporadic microsatellite instability-high colon cancers rarely display immunohistochemical evidence of Wnt signaling activation. Am J Surg Pathol 2015; 39: 313–317. [PubMed: 25602793]

75. Aoki K, Taketo MM. Adenomatous polyposis coli (APC): a multi-functional tumor suppressor gene. J Cell Sci 2007; 120: 3327–3335. [PubMed: 17881494]

76. Fodde R The APC gene in colorectal cancer. European journal of cancer 2002; 38: 867–871. [PubMed: 11978510]

77. Powell SM, Zilz N, Beazer-Barclay Y, Bryan TM, Hamilton SR, Thibodeau SN et al. APC mutations occur early during colorectal tumorigenesis. Nature 1992; 359: 235–237. [PubMed: 1528264]

78. Eto T, Miyake K, Nosho K, Ohmuraya M, Imamura Y, Arima K et al. Impact of loss-of-function mutations at the RNF43 locus on colorectal cancer development and progression. J Pathol 2018; 245: 445–455. [PubMed: 29756208]

79. Giannakis M, Hodis E, Jasmine Mu X, Yamauchi M, Rosenbluh J, Cibulskis K et al. RNF43 is frequently mutated in colorectal and endometrial cancers. Nat Genet 2014; 46: 1264–1266. [PubMed: 25344691]

80. Yagyu R, Furukawa Y, Lin YM, Shimokawa T, Yamamura T, Nakamura Y. A novel oncoprotein RNF43 functions in an autocrine manner in colorectal cancer. Int J Oncol 2004; 25: 1343–1348. [PubMed: 15492824]

81. Aaltonen LA, Peltomaki P, Leach FS, Sistonen P, Pylkkanen L, Mecklin JP et al. Clues to the pathogenesis of familial colorectal cancer. Science 1993; 260: 812–816. [PubMed: 8484121]

82. Ionov Y, Peinado MA, Malkhosyan S, Shibata D, Perucho M. Ubiquitous somatic mutations in simple repeated sequences reveal a new mechanism for colonic carcinogenesis. Nature 1993; 363: 558–561. [PubMed: 8505985]

83. Thibodeau SN, Bren G, Schaid D. Microsatellite instability in cancer of the proximal colon. Science 1993; 260: 816–819. [PubMed: 8484122]

84. Mizuno T, Cloyd JM, Vicente D, Omichi K, Chun YS, Kopetz SE et al. SMAD4 gene mutation predicts poor prognosis in patients undergoing resection for colorectal liver metastases. Eur J Surg Oncol 2018; 44: 684–692. [PubMed: 29551247]

85. Papageorgis P, Cheng K, Ozturk S, Gong Y, Lambert AW, Abdolmaleky HM et al. Smad4 inactivation promotes malignancy and drug resistance of colon cancer. Cancer Res 2011; 71: 998–1008. [PubMed: 21245094]

86. O'Rourke KP, Loizou E, Livshits G, Schatoff EM, Baslan T, Manchado E et al. Transplantation of engineered organoids enables rapid generation of metastatic mouse models of colorectal cancer. Nat Biotechnol 2017; 35: 577–582. [PubMed: 28459450]

87. Jeng MH, Jordan VC. Growth stimulation and differential regulation of transforming growth factor-beta 1 (TGF beta 1), TGF beta 2, and TGF beta 3 messenger RNA levels by norethindrone in MCF-7 human breast cancer cells. Mol Endocrinol 1991; 5: 1120–1128. [PubMed: 1834933]

88. Markowitz S, Wang J, Myeroff L, Parsons R, Sun L, Lutterbaugh J et al. Inactivation of the type II TGF-beta receptor in colon cancer cells with microsatellite instability. Science 1995; 268: 1336–1338. [PubMed: 7761852]

89. Alberici P, Gaspar C, Franken P, Gorski MM, de Vries I, Scott RJ et al. Smad4 haploinsufficiency: a matter of dosage. Pathogenetics 2008; 1: 2. [PubMed: 19014666]

90. Alberici P, Jagmohan-Changur S, De Pater E, Van Der Valk M, Smits R, Hohenstein P et al. Smad4 haploinsufficiency in mouse models for intestinal cancer. Oncogene 2006; 25: 1841–1851. [PubMed: 16288217]

91. Sakai E, Nakayama M, Oshima H, Kouyama Y, Niida A, Fujii S et al. Combined Mutation of Apc, Kras, and Tgfbr2 Effectively Drives Metastasis of Intestinal Cancer. Cancer Res 2018; 78: 1334–1346. [PubMed: 29282223]

92. Cerami E, Gao J, Dogrusoz U, Gross BE, Sumer SO, Aksoy BA et al. The cBio cancer genomics portal: an open platform for exploring multidimensional cancer genomics data. Cancer Discov 2012; 2: 401–404. [PubMed: 22588877]

93. Robinson JT, Thorvaldsdottir H, Wenger AM, Zehir A, Mesirov JP. Variant Review with the Integrative Genomics Viewer. Cancer Res 2017; 77: e31–e34. [PubMed: 29092934]

94. Robinson JT, Thorvaldsdottir H, Winckler W, Guttman M, Lander ES, Getz G et al. Integrative genomics viewer. Nat Biotechnol 2011; 29: 24–26. [PubMed: 21221095]

95. Sato T, Vries RG, Snippert HJ, van de Wetering M, Barker N, Stange DE et al. Single Lgr5 stem cells build crypt-villus structures in vitro without a mesenchymal niche. Nature 2009; 459: 262–265. [PubMed: 19329995]

96. Xue X, Shah YM. In vitro organoid culture of primary mouse colon tumors. J Vis Exp 2013: e50210. [PubMed: 23711911]

97. Li H, Durbin R. Fast and accurate short read alignment with Burrows-Wheeler transform. Bioinformatics 2009; 25: 1754–1760. [PubMed: 19451168]

98. Van der Auwera GA, Carneiro MO, Hartl C, Poplin R, Del Angel G, Levy-Moonshine A et al. From FastQ data to high confidence variant calls: the Genome Analysis Toolkit best practices pipeline. Curr Protoc Bioinformatics 2013; 43: 11 10 11–11 10 33. [PubMed: 25431634]

99. Lange S, Engleitner T, Mueller S, Maresch R, Zwiebel M, Gonzalez-Silva L et al. Analysis pipelines for cancer genome sequencing in mice. Nat Protoc 2020; 15: 266–315. [PubMed: 31907453]

100. Afgan E, Baker D, van den Beek M, Blankenberg D, Bouvier D, Cech M et al. The Galaxy platform for accessible, reproducible and collaborative biomedical analyses: 2016 update. Nucleic Acids Res 2016; 44: W3–W10. [PubMed: 27137889]

101. McLaren W, Gil L, Hunt SE, Riat HS, Ritchie GR, Thormann A et al. The Ensembl Variant Effect Predictor. Genome Biol 2016; 17: 122. [PubMed: 27268795]

Author Manuscript
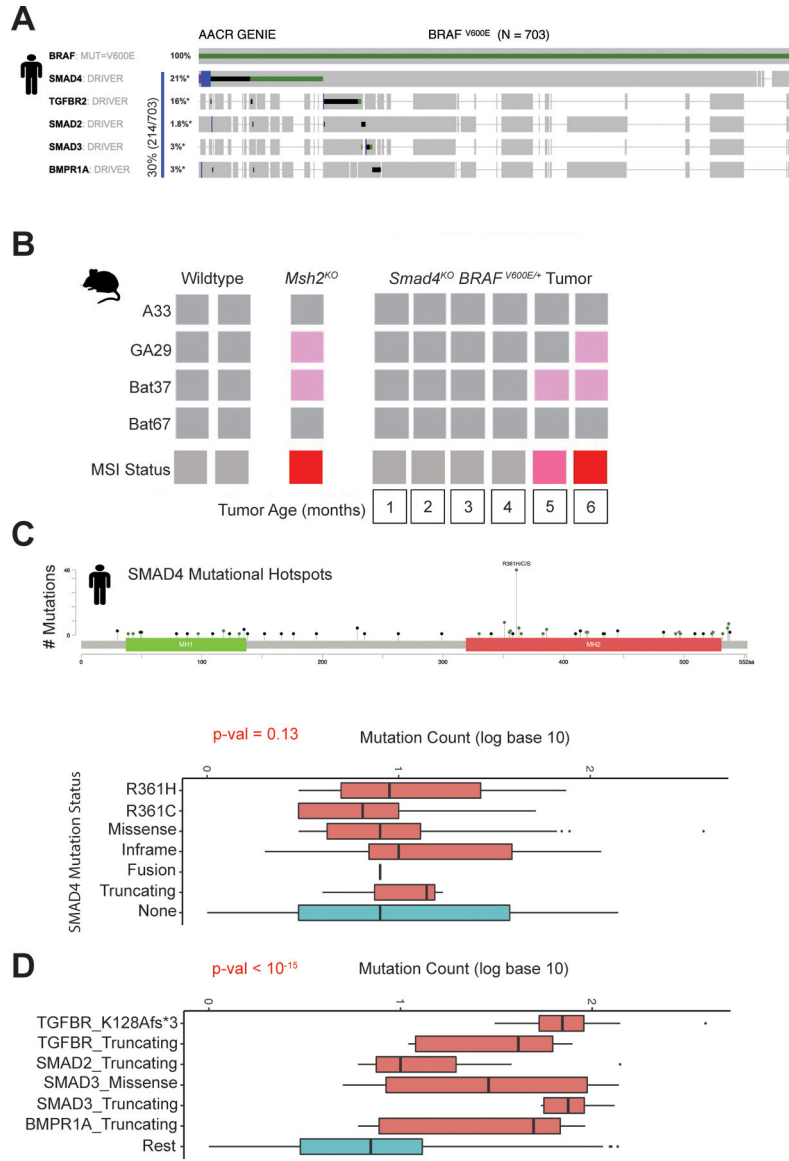
Author Manuscript

Author Manuscript

Author Manuscript

Figure 1: Loss of S*MAD4* Promotes Microsatellite Stable (MSS) Tumors.
(A) 30% of human tumors with *BRAF*^{V600E} mutation have one or more oncogenic alterations in TGFβ pathways, with predominant mutation being truncation (black) or missense (green) in *SMAD4*. (B) MSI analysis of Wildtype, *Msh2*^{KO}, and *Smad4*^{KO} *BRAF*$^{V600E/+}$ *Villin-Cre* mice organoids. Microsatellite loci (A33, GA29, Bat37, Bat67) were assessed as either unchanged (gray box) or experienced a genetic shift (pink box) in tumor organoids when compared to matched genomic tail DNA. MSI status dictated by number of genetic shifts (MSS = grey, MSI-L = pink, MSI-Hi = Red). (C) Analysis of human patients with *BRAF*^{V600E} colorectal cancer (from AACR GENIE) shows that tumors with oncogenic alteration in *SMAD4* have low mutation burden and are therefore most likely MSS. Red/blue boxes: *BRAF*^{V600E} cases with/without oncogenic alteration in *SMAD4*. (D) Similar analysis shows that *BRAF*^{V600E} tumors known to have an oncogenic mutation in other TGFβ pathway genes have almost an order of magnitude higher mutation

burden than the remaining $BRAF^{V600E}$ tumors and are therefore most likely MSI. Red/blue boxes: $BRAF^{V600E}$ cases known/not known to have an oncogenic mutation in *TGFBR2/SMAD2/SMAD3/BMPR1A* (p-val $< 10^{-15}$, 2-sided Wilcoxon rank-sum test).
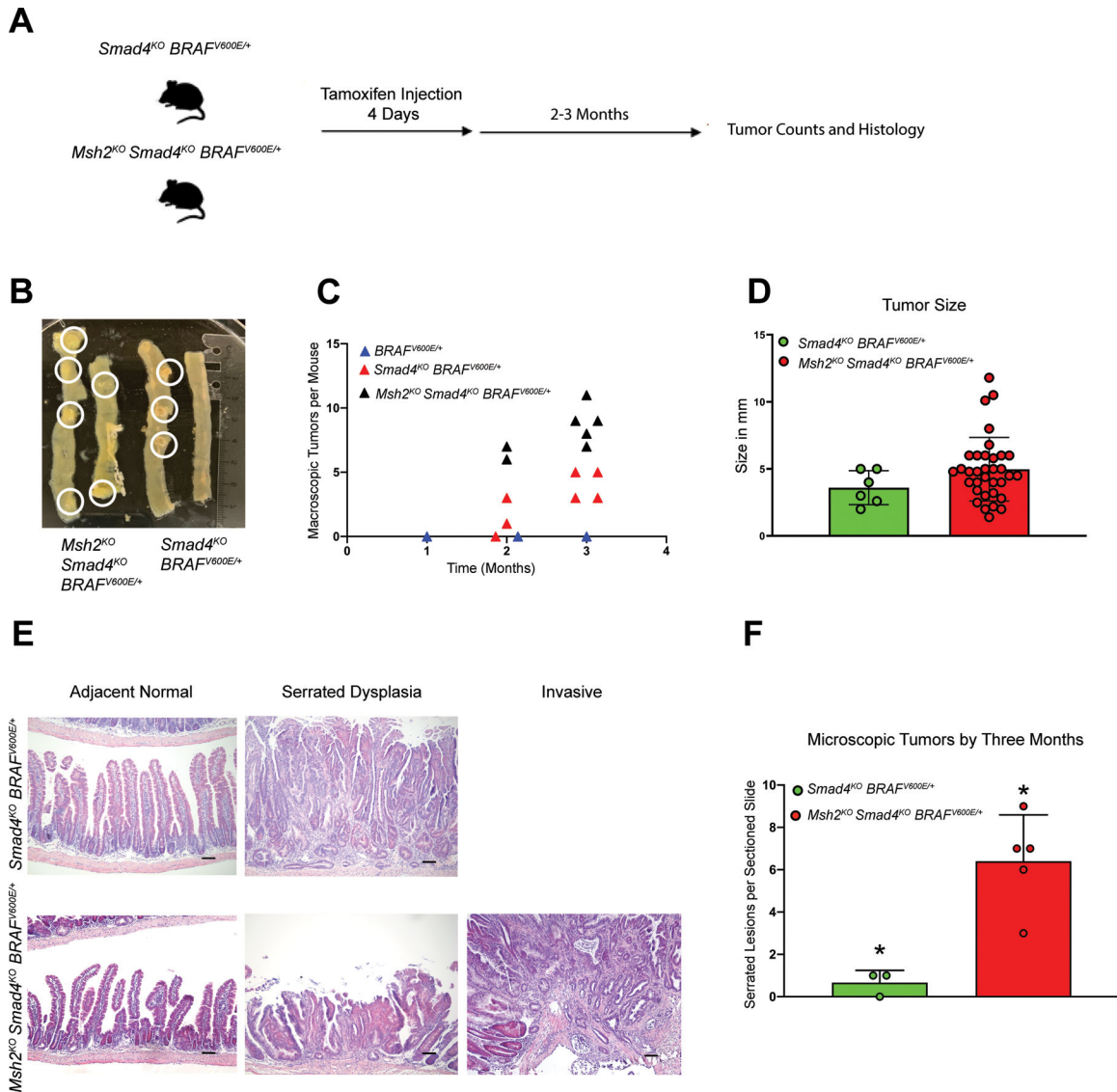
Figure 2: MSI Accelerates Serrated Tumorigenesis in $Smad4^{KO}$ $BRAF^{V600E/+}$ Environment.
(A) Mice were treated with tamoxifen for 4 consecutive days and then aged for 2–3 months post-injection. (B) Whole mount of $Msh2^{KO}$ $Smad4^{KO}$ $BRAF^{V600E/+}$ and $Smad4^{KO}$ $BRAF^{V600E/+}$ showing visible macroscopic tumors in duodenum and jejunum. (C) Counts of macroscopic tumors were based off 7 biological replicates of $Msh2^{KO}$ $Smad4^{KO}$ $BRAF^{V600E/+}$, $Smad4^{KO}$ $BRAF^{V600E/+}$ and 3 biological replicates of $BRAF^{V600E/+}$ as a control within 3 months post tamoxifen treatment. The number of macroscopic tumors found within the $Msh2^{KO}$ $Smad4^{KO}$ $BRAF^{V600E/+}$ mice are higher than in the $Smad4^{KO}$ $BRAF^{V600E/+}$ mice (p-val = 0.1055, Student's T-Test). (D) Size of tumors in $Msh2^{KO}$ $Smad4^{KO}$ $BRAF^{V600E/+}$ and $Smad4^{KO}$ $BRAF^{V600E/+}$. (E) H&E of $Smad4^{KO}$ $BRAF^{V600E/+}$ and $Msh2^{KO}$ $Smad4^{KO}$ $BRAF^{V600E/+}$. Images are representative of 3 biological replicates (Scale bar = 0.5mm). Low-grade and high-grade dysplasias were both noted and together classified as dysplasia, as compared with invasive cancer and normal tissue. (F) Counts of microscopic tumors were based off 3 biological replicates of $Msh2^{KO}$ $Smad4^{KO}$

$BRAF^{V600E/+}$ and $Smad4^{KO}$ $BRAF^{V600E/+}$ mice. The number of microscopic tumors found within the $Msh2^{KO}$ $Smad4^{KO}$ $BRAF^{V600E/+}$ mice are higher than in the $Smad4^{KO}$ $BRAF^{V600E/+}$ mice. (* = p-val = 0.005, Student's T-Test).
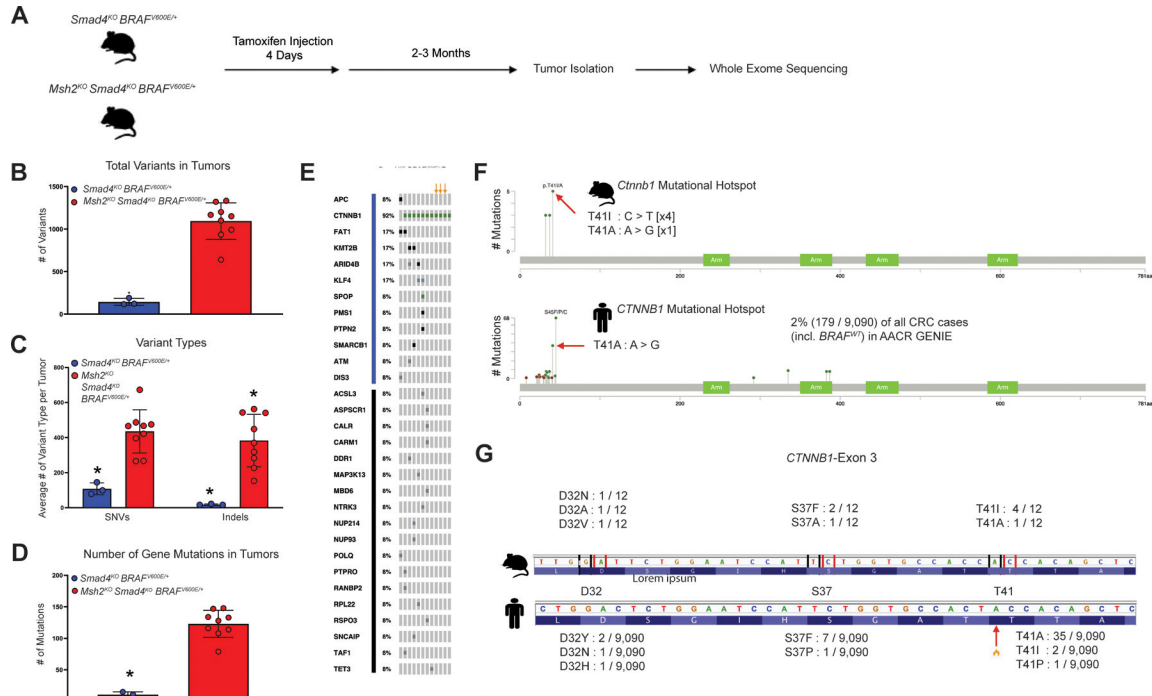
Figure 3: MSI Increases Mutational Burden, but there is Strong Selection for Oncogenic WNT Activation.

(A) Mice were treated with tamoxifen for 4 consecutive days and aged for 2–3 months post-injection. $Msh2^{KO} Smad4^{KO} BRAF^{V600E/+}$ (n=9) and $Smad4^{KO} BRAF^{V600E/+}$ (n=3) tumor organoids were submitted for whole exome sequencing along with matched genomic tail DNA. (B) Mutect2 analysis reveals $Msh2^{KO} Smad4^{KO} BRAF^{V600E/+}$ tumors have increased total variants (* = p-val < 0.0001, Student's T-Test). (C) Stratification of variants show higher frequencies of both Single Nucleotide Variants (SNVs) and Insertion/Deletion events (Indels) in $Msh2^{KO} Smad4^{KO} BRAF^{V600E/+}$ tumors (* = p-val = 0.0218, Student's T-Test). (D) $Msh2^{KO} Smad4^{KO} BRAF^{V600E/+}$ tumors also have more mutations within coding regions of genes (* = p-val < 0.0001, Student's T-Test). (E) Analysis of documented oncogenic mutations in either $Msh2^{KO} Smad4^{KO} BRAF^{V600E/+}$ or $Smad4^{KO} BRAF^{V600E/+}$ (orange arrows) tumors revealed that the most common oncogenic mutation in $Msh2^{KO} Smad4^{KO} BRAF^{V600E/+}$ and the only oncogenic mutation in $Smad4^{KO} BRAF^{V600E/+}$ was $CTNNB1$. Blue bar: oncogenic mutations according to OncoKB, black bar: truncating mutations in other cancer genes. (F) Oncogenic $Ctnnb1$ mutations identified in mouse tumors (top) coincide with $CTNNB1$ "hotspot" mutations in human patient cases (bottom). (G) Oncogenic $Ctnnb1$ mutations were isolated to Exon 3, with the most frequent point of mutation at "hotspot" T41.
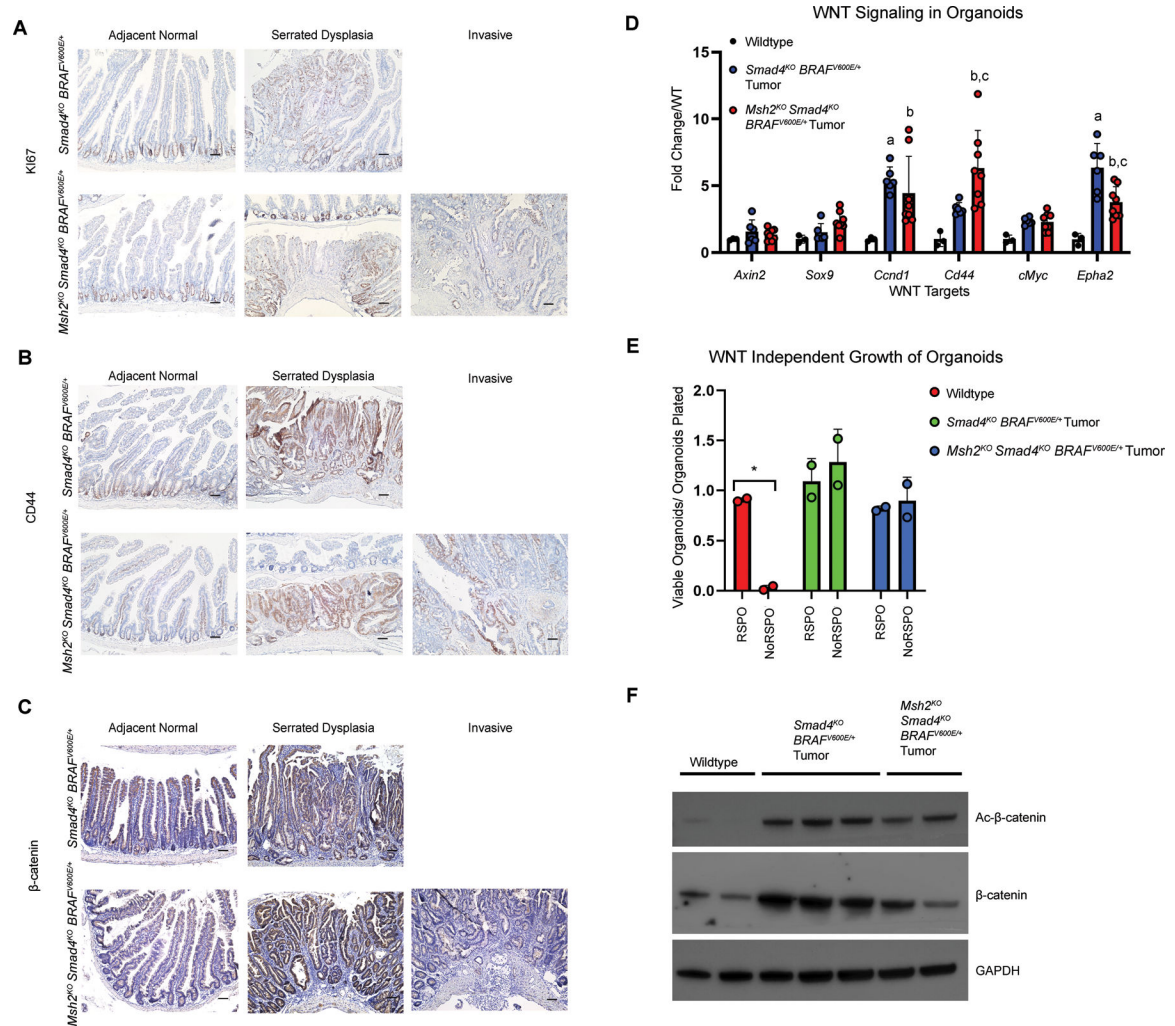
Figure 4: $Smad4^{KO}$ $BRAF^{V600E/+}$ Tumors Exhibit Elevated WNT Signaling.
$Smad4^{KO}$ $BRAF^{V600E/+}$ and $Msh2^{KO}$ $Smad4^{KO}$ $BRAF^{V600E/+}$ mice were collected 3 months post tamoxifen treatment. (A) Ki67 of adjacent normal and tumors show increased proliferation that extend beyond crypt compartments in tumors. Images are representative of three biological replicates. (B-C) CD44 and β-catenin of adjacent normal and tumors reveal higher WNT signaling in tumors. Images are representative of 3 biological replicates. (Scale bar = 0.5mm). Low-grade and high-grade dysplasias were both noted and together classified as dysplasia, as compared with invasive cancer and normal tissue. (D) qPCR analysis of WNT target genes in wildtype (n=3), $Smad4^{KO}$ $BRAF^{V600E/+}$ tumor (n=6), and $Msh2^{KO}$ $Smad4^{KO}$ $BRAF^{V600E/+}$ tumor (n=8) organoids. Results were normalized to gene expression of wildtype organoids (a = wildtype vs. $Smad4^{KO}$ $BRAF^{V600E/+}$ tumor, p-val < 0.05, b = wildtype vs. $Msh2^{KO}$ $Smad4^{KO}$ $BRAF^{V600E/+}$ tumor, p-val < 0.05, c = $Smad4^{KO}$ $BRAF^{V600E/+}$ tumor vs. $Msh2^{KO}$ $Smad4^{KO}$ $BRAF^{V600E/+}$ tumor, p-val < 0.05, two-way ANOVA). (E) Viability of wildtype (n=2), $Smad4^{KO}$ $BRAF^{V600E/+}$ tumor (n=2), and $Msh2^{KO}$ $Smad4^{KO}$ $BRAF^{V600E/+}$ tumor (n=2) organoids after 7 days cultured in media +/- R-Spondin (RSPO). Organoids were passaged and cultured for 2 days in complete media prior to removal of RSPO (* = p-val = 0.0107, two-way ANOVA). (F) Immunoblot of

wildtype (n=2), $Smad4^{KO}$ $BRAF^{V600E/+}$ tumor (n=3), and $Msh2^{KO}$ $Smad4^{KO}$ $BRAF^{V600E/+}$ tumor (n=2).
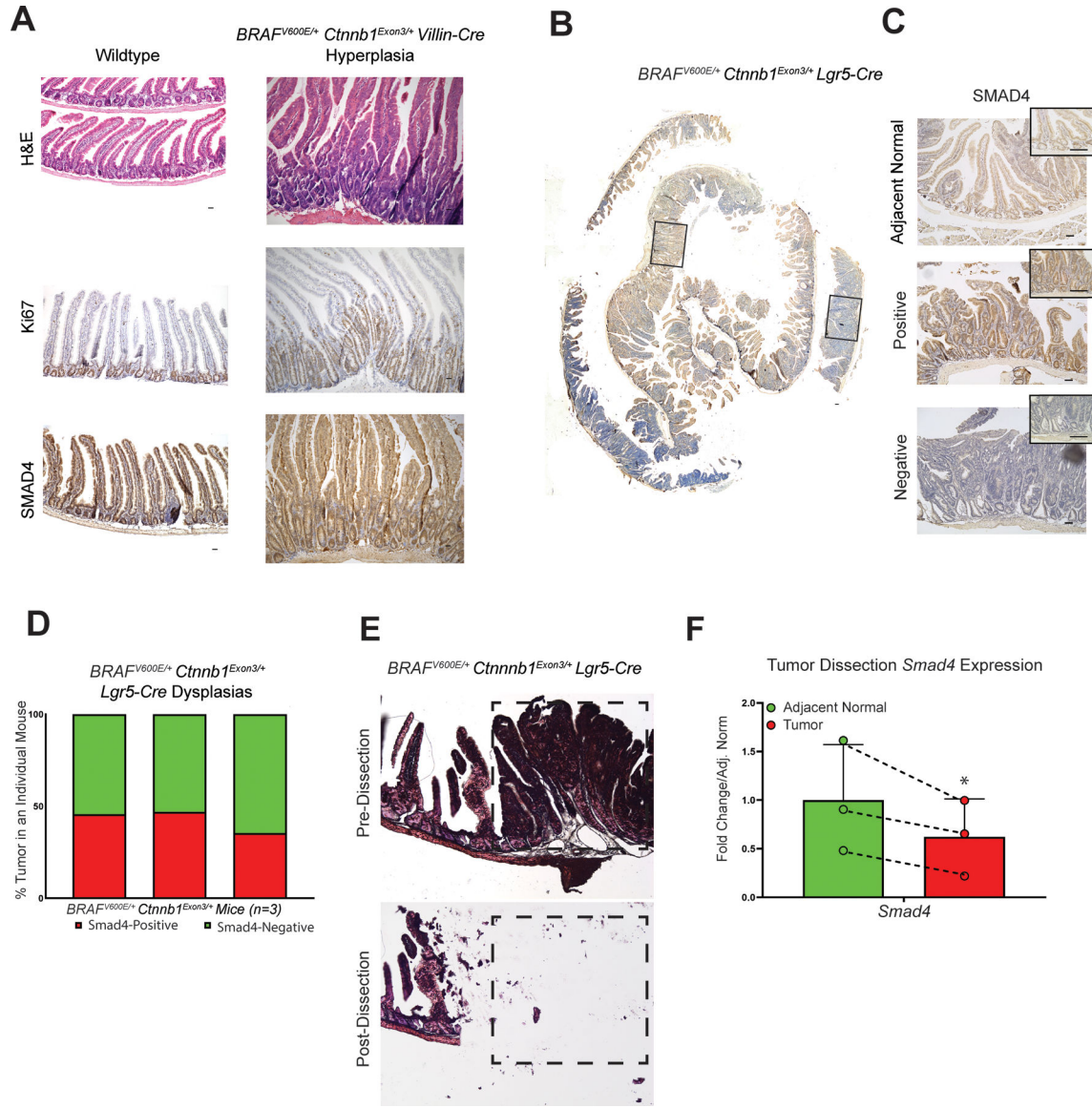
Figure 5: Loss of *Smad4* is Key Step in Serrated Hyperplasia-to-Dysplasia Transition.
(A) Histology of wildtype and *BRAF*$^{V600E/+}$ *Ctnnb1*$^{Exon3/+}$ *Villin-Cre* mice treated with tamoxifen for 4 consecutive days to induce recombination in the intestinal epithelium. Mice were collected 6 days post tamoxifen treatment based on weight loss. H&E and histology of Ki67 and SMAD4 of wildtype normal epithelium and *BRAF*$^{V600E/+}$ *Ctnnb1*$^{Exon3/+}$ *Villin-Cre* mice. Images are representative of 4 biological replicates. (Scale bar = 0.5mm). (B) *BRAF*$^{V600E/+}$ *Ctnnb1*$^{Exon3/+}$ *Lgr5-Cre* mice treated with tamoxifen to induce recombination in the stem cells of the intestinal epithelium. Mice were collected 2 months post tamoxifen treatment based on weight loss. Whole swiss roll of a SMAD4 stained *BRAF*$^{V600E/+}$ *Ctnnb1*$^{Exon3/+}$ *Lgr5-Cre* mouse. Images are representative of 3 biological replicates. (C) SMAD4 immunohistochemistry of *BRAF*$^{V600E/+}$ *Ctnnb1*$^{Exon3/+}$ *Lgr5-Cre* mice reveal both SMAD4-positive and SMAD4-negative dysplasias. Images are representative of 3 biological replicates. (Scale bars=0.5mm). (D) Distribution of SMAD-positive and SMAD4-negative

dysplasias found in $BRAF^{V600E/+}$ $Ctnnb1^{Exon3/+}$ $Lgr5$-Cre mice (n=3). (E) $BRAF^{V600E/+}$ $Ctnnb1^{Exon3/+}$ $Lgr5$-Cre dysplasias were dissected from adjacent tissue and extracted for RNA. (F) $Smad4$ expression is reduced in dissected tumors (n=4) when compared to paired adjacent tissue (* = p-val = 0.0477 Student's T-Test).
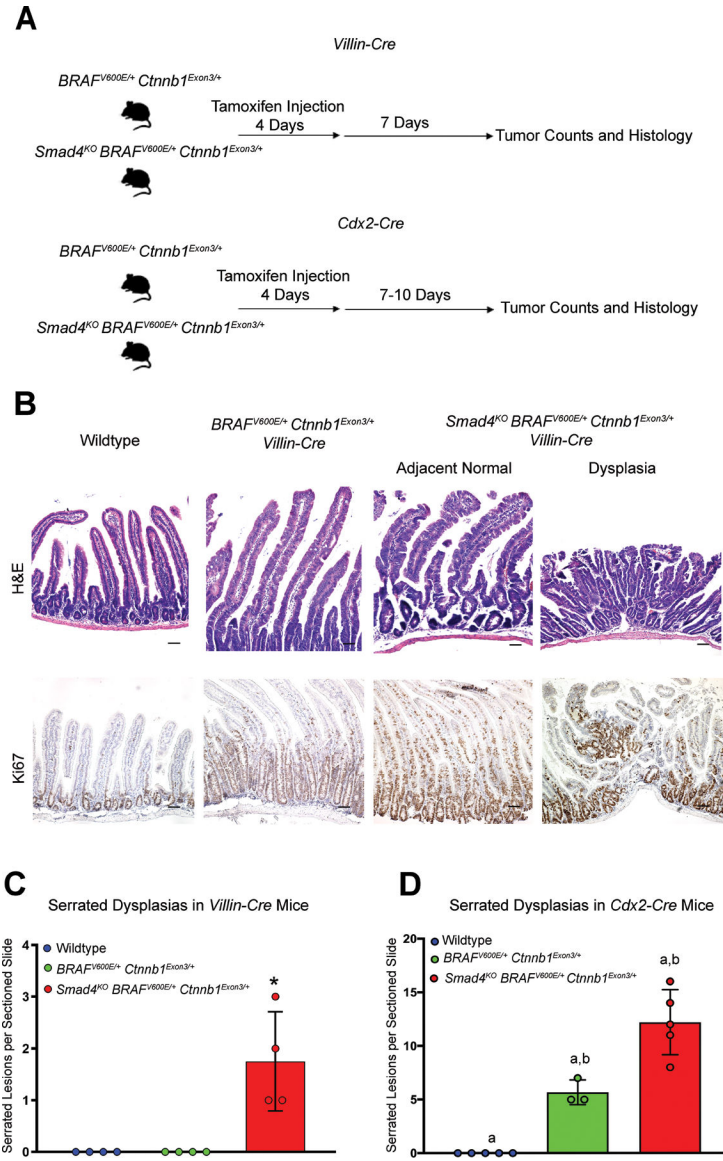
Figure 6: Activation of WNT in $Smad4^{KO}$ $BRAF^{V600E/+}$ Mouse Model Accelerates Serrated Tumorigenesis.

(A) Mice were treated with tamoxifen for 4 consecutive days and collected 7–10 days post-injection. (B) Histology of wildtype, $BRAF^{V600E/+}$ $Ctnnb1^{Exon3/+}$, and $Smad4^{KO}$ $BRAF^{V600E/+}$ $Ctnnb1^{Exon3/+}$ *Villin-Cre* mice. H&E and Ki67 revealed dysplasias in only the triple mutant model. Images are representative of 4 biological replicates. (Scale bar=0.5mm). (C) Counts of serrated dysplasias in *Villin-Cre* mice were based on 4 biological replicates of wildtype, $BRAF^{V600E/+}$ $Ctnnb1^{Exon3/+}$ and $Smad4^{KO}$ $BRAF^{V600E/+}$ $Ctnnb1^{Exon3/+}$ within 3 days post tamoxifen treatment (* = p-val = 0.0004 two-way ANOVA). (D) Counts of serrated dysplasias in wildtype (n = 5), $BRAF^{V600E/+}$ $Ctnnb1^{Exon3/+}$ (n = 3), and $Smad4^{KO}$ $BRAF^{V600E/+}$ $Ctnnb1^{Exon3/+}$ (n = 5) *Cdx2-Cre* mice within 10 days post tamoxifen treatment (a = p-val < 0.05 vs. control; b = p-val < 0.05 vs. $BRAF^{V600E/+}$ β-catenin$^{Exon3/+}$, two-way ANOVA).
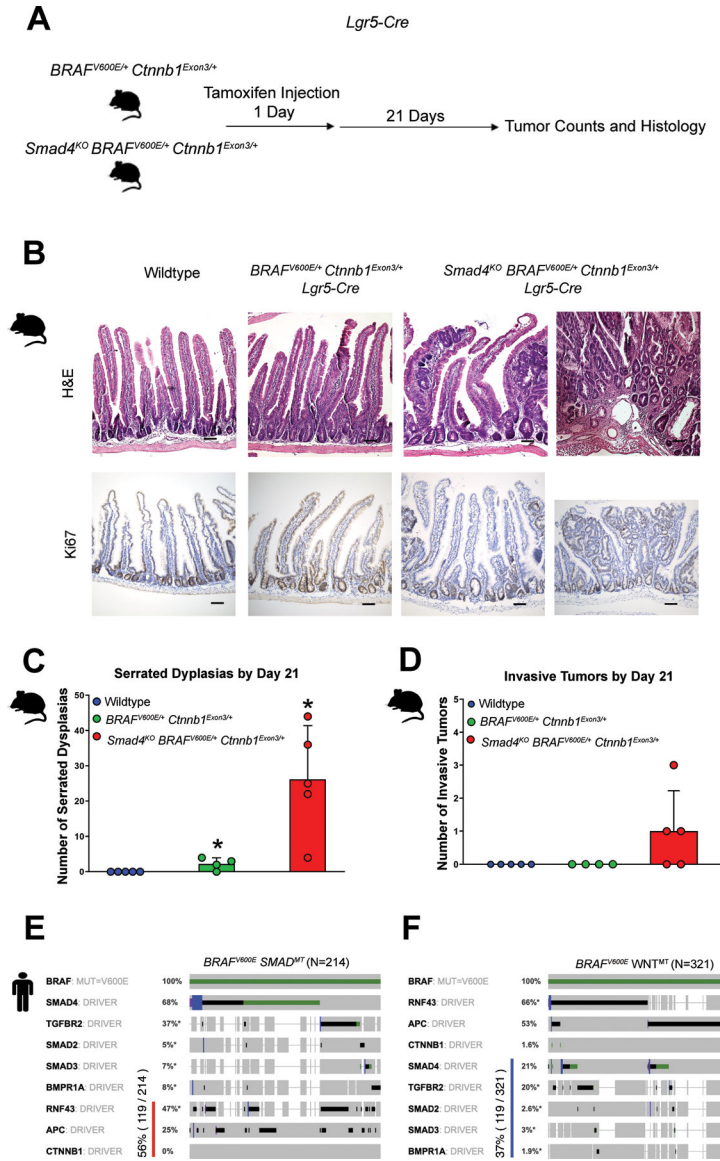
Figure 7: Activation of WNT in a *Smad4^KO^ BRAF^V600E/+^* Mouse Model Accelerates Serrated Tumorigenesis and Progression.

(A) Mice were injected with tamoxifen for 1 day and aged for 21 days post-injection. (B) Histology of wildtype, *BRAF^V600E/+^ Ctnnb1^Exon3/+^*, and *Smad4^KO^ BRAF^V600E/+^ Ctnnb1^Exon3/+^ Lgr5-Cre* mice treated with tamoxifen to induce recombination in the stem cells of the intestinal epithelium. H&E and Ki67 of the duodenum and dysplasias were identified. Images are representative of 3 biological replicates. (Scale bar=0.5mm). (C) Counts of serrated dysplasias in *Lgr5-Cre* mice within 21 days post tamoxifen treatment. (* = p-val = 0.0175, Student's T-Test). (D) Counts of invasive tumors in *Lgr5-Cre* mice were based on 5 biological replicates of wildtype, and *BRAF^V600E/+^ Ctnnb1^Exon3/+^* (n=4), and *Smad4^KO^ BRAF^V600E/+^ Ctnnb1^Exon3/+^* mice (p-val = 0.0945, one-way ANOVA). (E) Human patient data reveals at least 56% of tumors with BRAF^V600E^ mutation and oncogenic TGFβ pathway alterations have one or more oncogenic alterations in the WNT pathway. (F) At

least 37% of tumors with $BRAF^{V600E}$ mutation and oncogenic WNT pathway alterations also had one or more oncogenic alterations in the TGFβ pathway.

A

| Genotype	Time to Formation of Dysplasias	Degree of Dysplasia Development
Villin-Cre		
$BRAF^{V600E/+}$	N/A*	N/A*
$Smad4^{KO}\ BRAF^{V600E/+}$	2-3 months	++
$Msh2^{KO}\ Smad4^{KO}\ BRAF^{V600E/+}$	2-3 months	+++
$BRAF^{V600E/+}\ Ctnnb1^{Exon3/+}$	N/A	N/A
$Smad4^{KO}\ BRAF^{V600E/+}\ Ctnnb1^{Exon3/+}$	7-10 days	+++
Cdx2-Cre		
$BRAF^{V600E/+}\ Ctnnb1^{Exon3/+}$	10-14 days	+
$Smad4^{KO}\ BRAF^{V600E/+}\ Ctnnb1^{Exon3/+}$	10-14 days	+++
Lgr5-Cre		
$BRAF^{V600E/+}\ Ctnnb1^{Exon3/+}$	2 months	+
$Smad4^{KO}\ BRAF^{V600E/+}\ Ctnnb1^{Exon3/+}$	21 days	+++

B
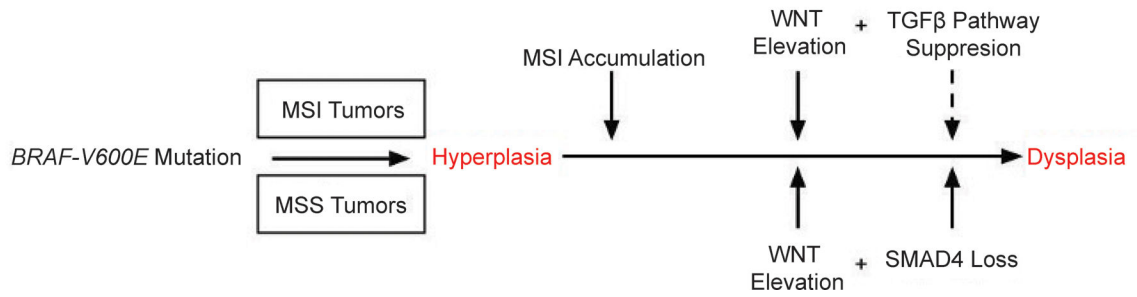
Figure 8: SMAD4/TGFβ Has Early-Stage Role in *BRAF-V600E* Serrated Tumor Progression.
(A) Summary of genotypes used in this study. Degree of dysplasia is ranked based upon average dysplasia counts per mouse relative to genotypes within Cre-specific drivers. Dysplasia formation and degree of dysplasia development reported is earliest timepoint recorded based upon this study. (* = dysplasias have been documented, but found at later timepoints)[9]. (B) Serrated cancers are predominantly driven by *BRAF-V600E* mutation. Loss of *SMAD4* or suppression of TGFβ pathway in combination with oncogenic WNT elevation promotes hyperplasia-to-dysplasia transition. *SMAD4* loss promotes the development of MSS serrated tumors, and *SMAD4* loss can occur before or after oncogenic elevation of WNT.